# Phase diagram of the anisotropic multichannel Kondo Hamiltonian revisited

Avraham Schiller[1] and Lorenzo De Leo[2]
[1]*Racah Institute of Physics, The Hebrew University, Jerusalem 91904, Israel*
[2]*Center for Materials Theory, Serin Physics Laboratory, Rutgers University, 136 Frelinghuysen Road, Piscataway, New Jersey 08854-8019, USA*

(Received 14 August 2007; published 14 February 2008)

The phase diagram of the multichannel Kondo Hamiltonian with an *XXZ* spin-exchange anisotropy is revisited, revealing a far richer fixed-point structure than previously appreciated. For a spin-$\frac{1}{2}$ impurity and $k>2$ conduction-electron channels, a second ferromagneticlike domain is found deep inside the antiferromagnetic regime. The new domain extends above a (typically large) critical longitudinal coupling $J_z^*>0$ and is separated from the antiferromagnetic domain by a second Kosterlitz-Thouless line. A similar line of stable ferromagneticlike fixed points with a residual isospin-$\frac{1}{2}$ local moment is shown to exist for large $J_z \gg |J_\perp| > 0$ and arbitrary $k$ and $s$ obeying $|k-2s|>1$. Here, $J_z$ is the longitudinal spin-exchange coupling, $J_\perp$ is the transverse coupling, and $s$ is the impurity spin. Near the free-impurity fixed point, spin-exchange anisotropy generates a highly relevant term for $s>1/2$ and arbitrary $k$. Depending on the sign of $J_z^2-J_\perp^2$ and the parity of $2s$, the system flows either to a conventional Fermi liquid with no residual degeneracy or to a $k$-channel, spin-$\frac{1}{2}$ Kondo effect or to a line of ferromagneticlike fixed points with a residual isospin-$\frac{1}{2}$ local moment. These results are obtained through a combination of perturbative renormalization-group techniques, Abelian bosonization, a strong-coupling expansion in $1/J_z$, and explicit numerical renormalization-group calculations.

DOI: 10.1103/PhysRevB.77.075114 PACS number(s): 72.15.Qm, 75.20.Hr

## I. INTRODUCTION AND OVERVIEW OF RESULTS

For over the last 40 years, the Kondo effect has occupied a central place in condensed-matter physics. While earlier studies of the effect have focused on its single-channel version realized in dilute magnetic alloys and valence-fluctuating systems, later attention has largely shifted to its more exotic multichannel variants where deviations from conventional Fermi-liquid behavior can be found. The overscreened Kondo effect is a paradigmatic example for quantum criticality in quantum-impurity systems. Besides the possible relevance to certain heavy fermion alloys,[1,2] ballistic metal point contacts,[3,4] scattering off two-level tunneling systems,[5–7] the charging of small metallic grains,[8,9] and transport in a modified single-electron transistor,[10] the overscreened Kondo effect is one of the rare examples of interaction-driven non-Fermi-liquid behavior that is well understood and well characterized theoretically.[11] The underscreened Kondo effect, which might be realized in ultrasmall quantum dots with an even number of electrons,[12] is a prototype for yet another form of unconventional behavior—that of a singular Fermi liquid.[13]

These vastly different ground states, as well as that of an ordinary Fermi liquid, can all be described within the single framework of the multichannel Kondo Hamiltonian, which is among the simplest yet richest models for strong electronic correlations in condensed-matter physics. The multichannel Kondo Hamiltonian presented in Eq. (3) describes the spin-exchange interaction of a spin-$s$ local moment with $k$ identical, independent bands of spin-$\frac{1}{2}$ electrons. For isotropic antiferromagnetic exchange, the low-energy physics features a subtle interplay between $k$ and $s$, which could be summarized as follows.[11] For $k=2s$, the impurity spin is exactly screened. A spin singlet progressively forms below a characteristic Kondo temperature $T_K$, signaling the formation of a local Fermi liquid. For $k>2s$, the impurity spin is overscreened by the $k$ conduction-electron channels. The system flows to an intermediate-coupling, non-Fermi-liquid fixed point, characterized by anomalous thermodynamic and dynamical properties. The elementary excitations are collective in nature, contradicting the notion of a Fermi liquid. For $k<2s$, the impurity spin is underscreened. The low-energy physics comprises of quasiparticle excitations plus a residual moment of size $s'=s-k/2$. It deviates, however, from a conventional Fermi liquid in the singular energy dependence of the scattering phase shift and the divergence of the quasiparticle density of states.[13–15] Such behavior was recently termed a singular Fermi liquid.[13] Similar qualitative behavior is found for ferromagnetic exchange with arbitrary $k$ and $s$, except that the residual moment has the full spin $s$.

Inherent to some of the leading scenarios for the realization of the multichannel Kondo model[5,6,8] is a large spin-exchange anisotropy. An *XXZ* anisotropy is well known to be irrelevant both in the single-channel ($k=1$, $s=1/2$) and in the two-channel ($k=2$, $s=1/2$) case. The accepted phase diagram for these two models consists of an antiferromagnetic and a ferromagnetic domain, separated by a Kosterlitz-Thouless line that traces the curve $J_z=-|J_\perp|$ at weak coupling. Here, $J_z$ and $J_\perp$ are the longitudinal and transverse exchange couplings, respectively. As long as one lies within the confines of the antiferromagnetic domain, the system flows to the isotropic spin-exchange fixed point regardless of how large the exchange anisotropy is.

Far less explored is the role of spin-exchange anisotropy for either $s>1/2$ or $k>2$. The stability of the overscreened fixed point against weak spin-exchange anisotropy was analyzed in Ref. 16 using conformal field theory. For $k>1$ and either $s=1/2$ or $s=(k-1)/2$, the non-Fermi-liquid fixed point was found to be stable against a weak spin-exchange anisotropy. In contrast, spin-exchange anisotropy was shown to be

 

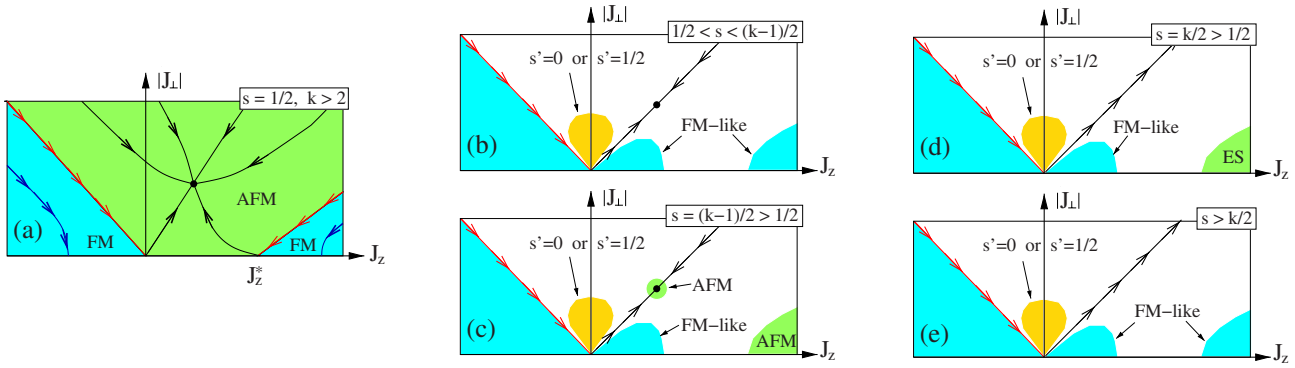


FIG. 1. (Color online) Phase diagram of the multichannel Kondo model for the different categories of $s$ and $k$. (a) $s=1/2$ and $k>2$. In addition to the well-established ferromagnetic (FM) domain for $J_z \leqslant -|J_\perp|$, a second ferromagneticlike domain extends to the right and below the diagonal red line stretching from $(J_z,J_\perp)=(J_z^*,0)$. Within bosonization, $J_z^*$ is given by Eq. (38). Each ferromagnetic-type domain is separated from the antiferromagnetic one by a Kosterlitz-Thouless line. (b) $1/2<s<(k-1)/2$. In addition to the conventional ferromagnetic domain for $J_z \leqslant -|J_\perp|$, the system flows to a line of stable ferromagneticlike fixed points with a residual isospin-$\frac{1}{2}$ local moment in two opposite limits: (i) for sufficiently small $J_z>|J_\perp|$ and (ii) for sufficiently large $J_z \gg |J_\perp|, D$ ($D$ being the conduction-electron bandwidth). For weak $|J_\perp|>|J_z|$, the system flows either to a Fermi-liquid fixed point with a frozen impurity (when $s$ is integer) or to an overscreened $k$-channel, spin-$\frac{1}{2}$ Kondo effect (when $s$ is half integer). The above weak-coupling behavior is generic to $s>1/2$. It extends to all cases described below, irrespective of $k$. (c) $s=(k-1)/2>1/2$. In contrast to (b), the isotropic overscreened fixed point, denoted by AFM, is stable against a weak spin-exchange anisotropy (i.e., in the vicinity of the overscreened fixed point). It is also unaffected by a sufficiently large $J_z \gg |J_\perp|, D$. (d) $s=k/2>1/2$. The exactly screened (ES) fixed point, corresponding to strong coupling, is unaffected by a sufficiently large anisotropy, $J_z \gg |J_\perp|, D$. However, it is unstable at weak coupling, as described above. (e) $s>k/2$. All underscreened cases flow to a line of stable ferromagneticlike fixed points with a residual isospin-$\frac{1}{2}$ local moment both for sufficiently large $J_z \gg |J_\perp|, D$ and for sufficiently small $J_z>|J_\perp|$.

a relevant perturbation at the overscreened fixed point for all other values of $1/2<s<(k-1)/2$ (assuming $k>4$; for $k=4$, it is a marginal perturbation),[16] though the nature of the anisotropic fixed points was never examined in detail. Another case largely unexplored is the effect of spin-exchange anisotropy on the underscreened fixed point for $s>k/2$. Indeed, the possibility of richer behavior for $s>1/2$ has recently emerged from the work of Konik *et al.*,[17] who noticed that a highly relevant term is generated at weak coupling when $|J_z| \neq |J_\perp|$. The ramifications of this term were only briefly touched upon in Ref. 17 for the particular case of $s=k=1$. It was discussed in greater detail for $k=1$ and general $s$ in the context of surface-induced anisotropy.[18]

In this paper, we revisit the phase diagram of the multichannel Kondo model with an *XXZ* spin-exchange anisotropy. We find a far more complex picture than previously appreciated, including new coupling regimes where an *XXZ* anisotropy substantially alters the low-energy physics. Our main findings can be summarized as follows.

(1) For $s=1/2$ and $k>2$, a second ferromagneticlike domain is found deep inside the antiferromagnetic regime. The new domain extends above a (typically large) critical longitudinal coupling $J_z^*>0$ and is separated from the conventional antiferromagnetic (non-Fermi-liquid) domain by a second Kosterlitz-Thouless line.

(2) For spin $s>1/2$ and arbitrary $k$, spin-exchange anisotropy generates a highly relevant term near the free-impurity fixed point.[17] The implications of this term are as follows. For sufficiently small $0<|\rho J_\perp|<|\rho J_z| \ll 1/ks$ ($\rho$ is the conduction-electron density of states per lattice site), the system flows to a line of stable ferromagneticlike fixed points with a residual isospin-$\frac{1}{2}$ moment. For sufficiently small $|\rho J_z|<|\rho J_\perp| \ll 1/ks$, the flow is either to a conventional Fermi liquid with no residual degeneracy (for integer $s$) or to a $k$-channel Kondo effect with an effective spin-$\frac{1}{2}$ local moment (for half integer $s$). Here, by sufficiently small $\rho J_z$ and $\rho J_\perp$ we mean the limit $J_z, J_\perp \to 0$ with any fixed ratio $r=J_z/J_\perp \neq \pm 1$. The closer $|r|$ is to 1, the smaller the couplings must be in order for these results to apply. The resulting weak-coupling phase diagram generalizes that of Ref. 17 from $s=k=1$ to arbitrary $s$ and $k$.

(3) For all $|k-2s|>1$, the system flows to a line of stable ferromagneticlike fixed points with a residual isospin-$\frac{1}{2}$ moment when $J_z \gg |J_\perp|>0$ is sufficiently large. Only for $k=2s$ and $k=2s+1$ are the exactly screened and overscreened fixed points unaffected by such a large anisotropy, which has the effect of introducing a marginal term when $k=2s-1$.

Here and throughout the paper, we use the generic term "ferromagneticlike" to indicate a low-energy fixed point where a residual local moment is left decoupled from the band.

A compilation of our results is presented in Fig. 1 in the form of phase diagrams for the different categories of $s$ and $k$. The phase diagrams for $s>1/2$ are still incomplete, as there remain extended coupling regimes where the low-energy physics is yet to be determined. We partially speculate about the behavior in these regimes at the end of the paper.

To obtain these results, we employ a combination of perturbative renormalization-group (RG) techniques, Abelian bosonization, a strong-coupling expansion in $1/J_z$, and explicit numerical renormalization-group[19] calculations. Using perturbative RG, we first analyze the limit of weak coupling in Sec. II. In addition to the standard RG equations for the

dimensionless couplings $\rho J_z$ and $\rho J_\perp$, a new Hamiltonian term proportional to $S_z^2$ is generated for $s>1/2$ and $J_z \neq J_\perp$.[17] Here, $S_z$ is the $z$ component of the impurity spin. Depending on the sign of $J_z^2-J_\perp^2$, the new Hamiltonian term favors either the maximally polarized impurity states ($S_z=\pm s$) or the minimally polarized ones. This leads to a qualitative difference between $J_z>|J_\perp|$ and $|J_\perp|>|J_z|$ and to the different low-temperature behaviors described above.

Proceeding with Abelian bosonization, we next show in Sec. III that the anisotropic multichannel Kondo Hamiltonian with $s=1/2$ and $k>1$ possesses an exact mapping between the two sets of coupling constants $(J_z,J_\perp)$ and $(J_z',J_\perp)$, where

$$\arctan\left(\frac{\pi\rho J_z'}{4}\right)=\frac{\pi}{k}-\arctan\left(\frac{\pi\rho J_z}{4}\right). \tag{1}$$

The above mapping is restricted to values of $J_z$ where the right-hand side of Eq. (1) does not exceed $\pi/2$. For $k=2$, this condition limits the validity of the mapping to $J_z \geqslant 0$, in which case Eq. (1) simplifies to

$$\rho J_z'=\left(\frac{4}{\pi}\right)^2\frac{1}{\rho J_z}. \tag{2}$$

For $k>2$, the mapping extends to negative values of $J_z$, relating $J_z>J_z^*=(4/\pi\rho)\tan(\pi/k)$ to $J_{\min}\leqslant J_z'<0$ and vice versa [see Eq. (37) for an explicit definition of $J_{\min}$]. Thus, in contrast to the single-channel and two-channel cases, the multichannel Kondo Hamiltonian with $s=1/2$ and $k>2$ possesses a line of stable ferromagneticlike fixed points for $J_z>J_z^*$. Note, however, that $J_z^*$ exceeds the bandwidth for intermediate values of $k$ and is pushed to weak coupling for $k\gg 1$.

Interestingly, the mapping of Eq. (1) is ingrained in the Anderson-Yuval approach to the multichannel Kondo problem, devised in Refs. 20 and 21. In fact, it was already recognized by Fabrizio *et al.* for $k=2$, (Ref. 20) but was never appreciated to our knowledge for $k>2$.[22] Here, we construct an explicit operator mapping between the two sets of model parameters applicable to arbitrary $k>1$.

Since the critical coupling $J_z^*$ predicted by Eq. (1) is typically larger than the bandwidth, one might question the applicability of bosonization with its unbounded linear dispersion. Could it be that $J_z^*\to\infty$ when the conduction electrons are placed on a lattice? To eliminate this concern, a strong-coupling expansion in $1/J_z$ is carried out in Secs. IV and V, first for $s=1/2$ and then for arbitrary $s$. The strong-coupling expansion not only confirms the existence of a new line of stable ferromagneticlike fixed points for $s=1/2$ and $k>2$ but further extends this result to arbitrary $s$ and $k$ obeying $|k-2s|>1$. For $k=2s$ and $k=2s+1$, the exactly screened and overscreened fixed points are shown to be unaffected by such a large anisotropy.

As an explicit demonstration of these ideas, the phase diagram of the $s=1/2$, $k=3$ model is studied in Sec. VI using Wilson's numerical renormalization-group (NRG) method.[19] The NRG results confirm the phase diagram inferred from Eq. (1), including the order of magnitude of the critical coupling $J_z^*$. An extension of the mapping of Eq. (1) to a spin-1 impurity is presented in turn in the Appendix. We conclude in Sec. VII with a discussion and summary of our results.

## II. WEAK COUPLING

We begin our discussion with the limit of weak coupling, which is treated using perturbative RG. In the standard notation, the multichannel Kondo Hamiltonian reads

$$\begin{aligned}\mathcal{H}=&\sum_{n=1}^{k}\sum_{\sigma=\uparrow,\downarrow}\sum_{\vec{k}}\epsilon_{\vec{k}}c_{\vec{k}n\sigma}^\dagger c_{\vec{k}n\sigma}\\&+\frac{J_z}{2N}\sum_{n=1}^{k}\sum_{\vec{k},\vec{k}'}[c_{\vec{k}n\uparrow}^\dagger c_{\vec{k}'n\uparrow}-c_{\vec{k}n\downarrow}^\dagger c_{\vec{k}'n\downarrow}]S_z\\&+\frac{J_\perp}{2N}\sum_{n=1}^{k}\sum_{\vec{k},\vec{k}'}[c_{\vec{k}n\uparrow}^\dagger c_{\vec{k}'n\downarrow}S^-+c_{\vec{k}n\downarrow}^\dagger c_{\vec{k}'n\uparrow}S^+].\end{aligned} \tag{3}$$

Here, $c_{\vec{k}n\sigma}^\dagger$ creates an electron with wave number $\vec{k}$ and spin projection $\sigma$ in the $n$th conduction-electron channel, $\vec{S}$ is a spin-$s$ operator, $J_z$ and $J_\perp$ are the longitudinal and transverse Kondo couplings, respectively, and $N$ is the number of lattice sites.

As a first step toward devising a perturbative RG treatment of the Hamiltonian of Eq. (3), we rewrite the model in a dimensionless form. To this end, we introduce the fermion operators

$$a_{\varepsilon n\sigma}^\dagger=\frac{1}{\sqrt{D\rho(E)N}}\sum_{\vec{k}}\delta\left(\varepsilon-\frac{\epsilon_{\vec{k}}}{D}\right)c_{\vec{k}n\sigma}^\dagger, \tag{4}$$

representing the $2k$ conduction-electron modes that couple to the impurity on the energy shell $E=\varepsilon D$. Here, $D$ is the conduction-electron bandwidth and $\rho(E)$ is the conduction-electron density of states per lattice site:

$$\rho(E)=\frac{1}{N}\sum_{\vec{k}}\delta(E-\epsilon_{\vec{k}}). \tag{5}$$

The dimensionless operators $a_{\varepsilon n\sigma}^\dagger$ have been normalized to obey canonical anticommutation relations

$$\{a_{\varepsilon n\sigma},a_{\varepsilon' n'\sigma'}^\dagger\}=\delta_{nn'}\delta_{\sigma\sigma'}\delta(\varepsilon-\varepsilon'). \tag{6}$$

Assuming a box density of states $\rho(E)=\rho\theta(D-|E|)$ and omitting all modes that decouple from the impurity, Eq. (3) is recast in the form $\mathcal{H}=D\tilde{\mathcal{H}}$, where $\tilde{\mathcal{H}}$ is the dimensionless Hamiltonian

$$\begin{aligned}\tilde{\mathcal{H}}=&\sum_{n=1}^{k}\sum_{\sigma=\uparrow,\downarrow}\int_{-1}^{1}\varepsilon a_{\varepsilon n\sigma}^\dagger a_{\varepsilon n\sigma}d\varepsilon\\&+\frac{\tilde{J}_z}{2}\sum_{n=1}^{k}\int_{-1}^{1}d\varepsilon\int_{-1}^{1}d\varepsilon'[a_{\varepsilon n\uparrow}^\dagger a_{\varepsilon' n\uparrow}-a_{\varepsilon n\downarrow}^\dagger a_{\varepsilon' n\downarrow}]S_z\\&+\frac{\tilde{J}_\perp}{2}\sum_{n=1}^{k}\int_{-1}^{1}d\varepsilon\int_{-1}^{1}d\varepsilon'[a_{\varepsilon n\uparrow}^\dagger a_{\varepsilon' n\downarrow}S^-+\text{H.c.}].\end{aligned} \tag{7}$$

Here, $\tilde{J}_z=\rho J_z$ and $\tilde{J}_\perp=\rho J_\perp$ are the dimensionless Kondo couplings.

Focusing on $|\tilde{J}_z|,|\tilde{J}_\perp|\ll 1/ks$, the Hamiltonian of Eq. (7) is treated using perturbative RG. The RG transformation consists of the following three steps. (i) Suppose that the bandwidth has already been lowered from its initial value $D$ to some value $D'=De^{-l}$ $(l>0)$. Further lowering the bandwidth to $D''=D'(1-\delta l)$ requires the elimination of all $a_{\varepsilon n\sigma}$ degrees of freedom in the interval $1-\delta l<|\varepsilon|\leq 1$. This goal is accomplished using Anderson's poor-man's scaling.[23] At the conclusion of this step, all integrations in Eq. (7) have been reduced to the range $-(1-\delta l)\leq x\leq 1-\delta l$. The RG transformation is completed by (ii) rescaling $\tilde{\mathcal{H}}\to\tilde{\mathcal{H}}/(1-\delta l)$ to account for the reduced bandwidth and (iii) restoring the original integration ranges in Eq. (7) by converting to

$$a_{\varepsilon n\sigma}\to\tilde{a}_{\varepsilon n\sigma}=(1-\delta l)^{1/2}a_{(1-\delta l)\varepsilon n\sigma}. \tag{8}$$

This latter step allows us to write

$$\int_{-(1-\delta l)}^{1-\delta l}a_{\varepsilon n\sigma}d\varepsilon=(1-\delta l)^{1/2}\int_{-1}^{1}\tilde{a}_{\varepsilon n\sigma}d\varepsilon. \tag{9}$$

The dimensionless Hamiltonian is recast in this manner in a self-similar form, but with renormalized couplings. These evolve according to a set of flow equations detailed below.

For $s=1/2$, we recover the familiar RG equations

$$\frac{d\tilde{J}_z}{dl}=\tilde{J}_\perp^2, \tag{10}$$

$$\frac{d\tilde{J}_\perp}{dl}=\tilde{J}_\perp\tilde{J}_z. \tag{11}$$

From these equations, one concludes that spin-exchange anisotropy is irrelevant for weak $\tilde{J}_z>-|\tilde{J}_\perp|$, regardless of the number of channels $k$. A different qualitative picture emerges when the spin $s$ exceeds one-half, as the highly relevant term $\tilde{\Delta}S_z^2$ is generated within $\tilde{\mathcal{H}}$.[17] Starting from zero, the coupling $\tilde{\Delta}$ renormalizes according to[17]

$$\frac{d\tilde{\Delta}}{dl}=\tilde{\Delta}-k\ln(2)[\tilde{J}_z^2-\tilde{J}_\perp^2], \tag{12}$$

which supplements Eqs. (10) and (11) for the renormalizations of $\tilde{J}_z$ and $\tilde{J}_\perp$. Restricting attention to $s>1/2$, we now analyze the ramifications of the new coupling generated as a function of $s$, $k$, and the bare Kondo couplings $J_z$ and $J_\perp$. Our analysis extends that of Ref. 17 from $s=k=1$ to arbitrary $k$ and $s>1/2$, revealing qualitative differences between integer and half integer $s$.

Since $\tilde{J}_z^2-\tilde{J}_\perp^2$ is conserved under the RG, a negative (positive) $\tilde{\Delta}$ is generated if the bare Kondo couplings satisfy $|J_z|>|J_\perp|$ $(|J_z|<|J_\perp|)$. For a given ratio $J_z/J_\perp\neq\pm 1$ and sufficiently small $|J_\perp|$, the coupling $|\tilde{\Delta}|$ approaches unity well before any Kondo temperature can be reached. This has the effect of freezing all but the lowest lying spin states. For $|J_z|>|J_\perp|$ (negative $\tilde{\Delta}$), only the maximally polarized states $S_z=\pm s$ are thus left. For $|J_z|<|J_\perp|$ (positive $\tilde{\Delta}$), the picture depends on the parity of $2s$. When $s$ is half integer, the two degenerate states $S_z=\pm 1/2$ are selected. When $s$ is integer, only the state $S_z=0$ remains.

Depending on the case realized, a different effective low-energy Hamiltonian applies. Consider first the case $|J_z|>|J_\perp|$ (negative $\tilde{\Delta}$). Introducing the isospin operators

$$\tau_z=\frac{1}{2}|s\rangle\langle s|-\frac{1}{2}|-s\rangle\langle -s|, \tag{13}$$

$$\tau^{\pm}=|\pm s\rangle\langle\mp s|, \tag{14}$$

the resulting low-energy Hamiltonian contains the term

$$\tilde{\mathcal{H}}_{J_z}=s\tilde{J}_z\sum_{n=1}^{k}\int_{-1}^{1}d\varepsilon\int_{-1}^{1}d\varepsilon'[a_{\varepsilon n\uparrow}^\dagger a_{\varepsilon' n\uparrow}-a_{\varepsilon n\downarrow}^\dagger a_{\varepsilon' n\downarrow}]\tau_z, \tag{15}$$

obtained by projecting the spin-exchange interaction term of Eq. (7) onto the $S_z=\pm s$ subspace. Here, $\tilde{J}_z$ is the running coupling constant at the scale where $|\tilde{\Delta}|$ approaches 1. In contrast to Eq. (15), terms that flip the isospin $\vec{\tau}$ involve the creation and annihilation of at least $2s$ conduction electrons. This follows from the fact that a flip in $\vec{\tau}$ changes $S_z$ by $\pm 2s$. Since the Hamiltonian conserves the total spin projection of the entire system (impurity plus conduction electrons), such a process must be accompanied by an opposite spin flip of $2s$ conduction electrons in the vicinity of the impurity. As a result, isospin-flip terms have the scaling dimension $\Delta_\perp\geq 2s\geq 2$ about the free-impurity fixed point, rendering these terms irrelevant. The resulting fixed-point structure corresponds then to a line of ferromagneticlike fixed points with a residual isospin-$\frac{1}{2}$ local moment, characterized by a finite $\tilde{J}_z$. Note that this picture is insensitive to the sign of the bare Kondo couplings. It equally applies to positive and negative $J$'s.

Proceeding to the case $|J_z|<|J_\perp|$ (positive $\tilde{\Delta}$), we first consider a half-integer spin. Here, the two states selected by $\tilde{\Delta}$ are $S_z=\pm 1/2$. Similar to Eqs. (13) and (14), we introduce the isospin representation

$$\tau_z=\frac{1}{2}\left[|1/2\rangle\langle 1/2|-|-1/2\rangle\langle -1/2|\right], \tag{16}$$

$$\tau^{\pm}=|\pm 1/2\rangle\langle\mp 1/2|, \tag{17}$$

which now pertains to the states $|S_z=\pm 1/2\rangle$. Projection of Eq. (7) onto the $S_z=\pm 1/2$ subspace yields the following effective spin-exchange interaction:

$$\tilde{\mathcal{H}}_J=\frac{\tilde{J}_z}{2}\sum_{n=1}^{k}\int_{-1}^{1}d\varepsilon\int_{-1}^{1}d\varepsilon'[a_{\varepsilon n\uparrow}^\dagger a_{\varepsilon' n\uparrow}-a_{\varepsilon n\downarrow}^\dagger a_{\varepsilon' n\downarrow}]\tau_z + \gamma\frac{\tilde{J}_\perp}{2}\sum_{n=1}^{k}\int_{-1}^{1}d\varepsilon\int_{-1}^{1}d\varepsilon'[a_{\varepsilon n\uparrow}^\dagger a_{\varepsilon' n\downarrow}\tau^- + \text{H.c.}], \tag{18}$$

with $\gamma=\sqrt{s(s+1)+1/4}\geq 2$ (recall that $s\geq 3/2$). Once again,

$\tilde{J}_z$ and $\tilde{J}_\perp$ in Eq. (18) are the running coupling constants at the scale where $\tilde{\Delta}$ approaches 1.

Equation (18) has the form of a $k$-channel Kondo Hamiltonian with an effective isospin-$\frac{1}{2}$ local moment. Importantly, since $|\tilde{J}_z| < \gamma|\tilde{J}_\perp| \ll 1$, one lies in the confines of the antiferromagnetic domain. Hence, irrespective of the original half-integer spin $s$, the system flows to the overscreened fixed point of the $k$-channel Kondo effect with spin $s'=1/2$. (For $k=1$, the flow is to the strong-coupling fixed point of the conventional one-channel Kondo effect). Excluding the case $s=k/2-1/2$ with antiferromagnetic spin exchange, the resulting low-energy physics differs markedly from that of the isotropic model, whether ferromagnetic or antiferromagnetic. Most strikingly, the underscreened fixed point for $J_z=J_\perp>0$ and $s>k/2>1/2$ is replaced with an overscreened fixed point for any given ratio $-1<J_z/J_\perp<1$ and sufficiently small $|J_\perp|$.

Of the different possible cases for $\tilde{\Delta}$ and $s$, the simplest picture is recovered for $|J_z|<|J_\perp|$ and integer $s$. Here, the impurity spin is frozen in the $S_z=0$ state, losing its dynamics. This results in a conventional Fermi-liquid fixed point with neither non-Fermi-liquid characteristics nor a residual local-moment degeneracy.

## III. EXACT MAPPING FOR $s=1/2$

Evidently, there is a qualitative difference between $s=1/2$ and $s>1/2$ when it comes to the effect of spin-exchange anisotropy in the weak-coupling limit. In this section, we focus on $s=1/2$ and extend our treatment of an $XXZ$ anisotropy to arbitrary $J_z$. Specifically, we use Abelian bosonization to derive the mapping of Eq. (1). Our starting point is the continuum-limit version of the multichannel Kondo Hamiltonian,

$$\begin{aligned}\mathcal{H} &= \sum_{n=1}^{k}\sum_{\sigma=\uparrow,\downarrow} i\hbar v_F \int_{-\infty}^{\infty} \psi_{n\sigma}^{\dagger}(x)\partial_x \psi_{n\sigma}(x)dx \\ &+ \sum_{n=1}^{k} \frac{J_\perp a}{2}[\psi_{n\downarrow}^{\dagger}(0)\psi_{n\uparrow}(0)S^{+} + S^{-}\psi_{n\uparrow}^{\dagger}(0)\psi_{n\downarrow}(0)] \\ &+ \sum_{n=1}^{k} \frac{J_z a}{2} S_z[\psi_{n\uparrow}^{\dagger}(0)\psi_{n\uparrow}(0) - \psi_{n\downarrow}^{\dagger}(0)\psi_{n\downarrow}(0)] - g_i h S_z \\ &- \frac{g_e h}{2}\sum_{n=1}^{k}\int_{-\infty}^{\infty}[\psi_{n\uparrow}^{\dagger}(x)\psi_{n\uparrow}(x) - \psi_{n\downarrow}^{\dagger}(x)\psi_{n\downarrow}(x)]dx, \quad (19)\end{aligned}$$

written in terms of the left-moving one-dimensional fields

$$\psi_{n\sigma}(x) = \frac{1}{\sqrt{2a}}\int_{-1}^{1} e^{-ix\varepsilon\pi/a} a_{\varepsilon n\sigma} d\varepsilon, \quad (20)$$

with $n=1,\ldots,k$ and $\sigma=\uparrow,\downarrow$. Here, $\vec{S}$ is a spin-$\frac{1}{2}$ operator, $a$ is a short-distance cutoff corresponding to a lattice spacing, $x$ is a fictitious coordinate conjugate to $k=\varepsilon\pi/a$, and $h$ is an applied magnetic field. For the sake of generality, we allow for different impurity and conduction-electron Landé $g$ factors, $g_i$ and $g_e$, respectively.

To treat the Hamiltonian of Eq. (19), we resort to Abelian bosonization. According to standard prescriptions,[24] $2k$ boson fields are introduced—one boson field $\Phi_{n\sigma}(x)$ for each left-moving fermion field $\psi_{n\sigma}(x)$. The fermion fields are written as

$$\psi_{n\sigma}(x) = P_{n\sigma}\frac{1}{\sqrt{2\pi\alpha}} e^{-i\Phi_{n\sigma}(x)}, \quad (21)$$

where the boson fields obey

$$[\Phi_{n\sigma}(x), \Phi_{n'\sigma'}(y)] = -i\delta_{nn'}\delta_{\sigma\sigma'}\pi\,\mathrm{sgn}(x-y). \quad (22)$$

The ultraviolet momentum cutoff $\alpha^{-1}=\pi/a$ is related to the conduction-electron bandwidth $D$ and the density of states per lattice site $\rho$ through $D=\hbar v_F/\alpha$ and $\rho=1/(2D)=\alpha/(2\hbar v_F)$, respectively. The operators $P_{n\sigma}$ in Eq. (21) are phase-factor operators. These come to ensure that the different fermion species anticommute. Our explicit choices for the phase-factor operators are

$$P_{n\sigma} = \exp\left(i\pi\left[N_{n\uparrow} + \sum_{j<n}\sum_{\sigma'} N_{j\sigma'}\right]\right), \quad (23)$$

where $N_{j\sigma}$ is the number operator for electrons with spin projection $\sigma$ in channel $j$.

In terms of the boson fields, the multichannel Kondo Hamiltonian takes the form

$$\begin{aligned}\mathcal{H} &= \sum_{n=1}^{k}\sum_{\sigma=\uparrow,\downarrow}\frac{\hbar v_F}{4\pi}\int_{-\infty}^{\infty}[\nabla\Phi_{n\sigma}(x)]^2 dx \\ &+ \sum_{n=1}^{k}\frac{J_\perp}{4}\{e^{i[\Phi_{n\uparrow}(0)-\Phi_{n\downarrow}(0)]}S^{-} + \mathrm{H.c.}\} \\ &+ \delta_z\frac{a}{\pi^2\rho}\sum_{n=1}^{k}[\nabla\Phi_{n\uparrow}(0) - \nabla\Phi_{n\downarrow}(0)]S_z - g_i h S_z \\ &- \frac{g_e h}{4\pi}\sum_{n=1}^{k}\int_{-\infty}^{\infty}[\nabla\Phi_{n\uparrow}(x) - \nabla\Phi_{n\downarrow}(x)]dx, \quad (24)\end{aligned}$$

where

$$\delta_z = \arctan\left(\frac{\pi\rho J_z}{4}\right) \quad (25)$$

is the phase shift associated with $J_z$ in the absence of $J_\perp$. Note that $\delta_z$ is bounded in magnitude by $\pi/2$, which stems from the cutoff scheme used in bosonization. Although the bosonic Hamiltonian of Eq. (24) does support larger values of $|\delta_z|$, this parameter must not exceed $\pi/2$ in order for the bosonic Hamiltonian to possess a fermionic counterpart of the form of Eq. (19). We shall return to this important point later on.

At this stage, we manipulate the bosonic Hamiltonian of Eq. (24) through a sequence of steps. We begin by converting to $2k$ new boson fields, consisting of

$$\Phi_s(x) = \frac{1}{\sqrt{2k}} \sum_{n=1}^{k} [\Phi_{n\uparrow}(x) - \Phi_{n\downarrow}(x)] \tag{26}$$

plus $2k-1$ orthogonal fields $\Phi_\mu(x)$, with $\mu=1,\ldots,2k-1$. The orthogonal fields $\Phi_\mu(x)$ are formally expressed as

$$\Phi_\mu(x) = \sum_{n=1}^{k} \sum_{\sigma=\uparrow,\downarrow} e_{n\sigma}^{\mu} \Phi_{n\sigma}(x), \tag{27}$$

where the real coefficients $e_{n\sigma}^{\mu}$ obey

$$\sum_{n=1}^{k} \sum_{\sigma=\uparrow,\downarrow} e_{n\sigma}^{\mu} e_{n\sigma}^{\nu} = \delta_{\mu\nu}, \tag{28}$$

$$\sum_{n=1}^{k} [e_{n\uparrow}^{\mu} - e_{n\downarrow}^{\mu}] = 0. \tag{29}$$

The precise form of the coefficients $e_{n\sigma}^{\mu}$ is of no practical importance to our discussion and need not concern us. Their choice is not unique. In terms of the new fields, the combinations $\Phi_{n\uparrow}(x)-\Phi_{n\downarrow}(x)$ take the form

$$\Phi_{n\uparrow}(x) - \Phi_{n\downarrow}(x) = \sqrt{\frac{2}{k}} \Phi_s(x) + \varphi_n(x), \tag{30}$$

where $\varphi_n(x)$ is some linear combination of the fields $\Phi_\mu(x)$ with $\mu=1,\ldots,2k-1$. Once again, the precise form of the $\varphi_n$'s is of no real significance to our discussion. We shall only rely on them being orthogonal to $\Phi_s(x)$.

Using the new boson fields defined above, the Hamiltonian of Eq. (24) is converted to

$$\mathcal{H} = \frac{\hbar v_F}{4\pi} \int_{-\infty}^{\infty} \left[ (\nabla\Phi_s)^2 + \sum_{\mu=1}^{2k-1} (\nabla\Phi_\mu)^2 \right] dx + \sum_{n=1}^{k} \frac{J_\perp}{4} \{ e^{i\sqrt{2/k}\Phi_s(0) + i\varphi_n(0)} S^- + \text{H.c.} \} + \delta_z \frac{a}{\pi^2\rho} \sqrt{2k}\, \nabla\Phi_s(0) S_z - g_i h S_z - \frac{g_e h}{4\pi} \sqrt{2k} \int_{-\infty}^{\infty} \nabla\Phi_s(x) dx. \tag{31}$$

Next, the canonical transformation $\mathcal{H}' = U\mathcal{H}U^\dagger$, with $U = \exp\left[ i\sqrt{\frac{8}{k}} \Phi_s(0) S_z \right]$, is applied to obtain

$$\mathcal{H}' = \frac{\hbar v_F}{4\pi} \int_{-\infty}^{\infty} \left[ (\nabla\Phi_s)^2 + \sum_{\mu=1}^{2k-1} (\nabla\Phi_\mu)^2 \right] dx + \sum_{n=1}^{k} \frac{J_\perp}{4} \{ e^{-i\sqrt{2/k}\Phi_s(0) + i\varphi_n(0)} S^- + \text{H.c.} \} + \left( \delta_z - \frac{\pi}{k} \right) \frac{a}{\pi^2\rho} \sqrt{2k}\, \nabla\Phi_s(0) S_z - (g_i - 2g_e) h S_z - \frac{g_e h}{4\pi} \sqrt{2k} \int_{-\infty}^{\infty} \nabla\Phi_s(x) dx. \tag{32}$$

Here, we have omitted a constant term from $\mathcal{H}'$ and made use of the identity $a/\pi\rho = 2\hbar v_F$ in writing the coefficient of $\nabla\Phi_s(0)S_z$. Finally, the transformation $\Phi_s(x) \to -\Phi_s(x)$ is applied, which yields

$$\mathcal{H}' = \frac{\hbar v_F}{4\pi} \int_{-\infty}^{\infty} \left[ (\nabla\Phi_s)^2 + \sum_{\mu=1}^{2k-1} (\nabla\Phi_\mu)^2 \right] dx + \sum_{n=1}^{k} \frac{J_\perp}{4} \{ e^{i\sqrt{2/k}\Phi_s(0) + i\varphi_n(0)} S^- + \text{H.c.} \} + \delta_z' \frac{a}{\pi^2\rho} \sqrt{2k}\, \nabla\Phi_s(0) S_z + (2g_e - g_i) h S_z + \frac{g_e h}{4\pi} \sqrt{2k} \int_{-\infty}^{\infty} \nabla\Phi_s(x) dx, \tag{33}$$

with $\delta_z' = \pi/k - \delta_z$.

The Hamiltonian of Eq. (33) is identical to that of Eq. (31), apart from the renormalization of certain parameters: $\delta_z \to \delta_z'$, $h \to -h$, and $g_i \to 2g_e - g_i$. As long as $|\delta_z'| \leq \pi/2$, one can reverse the series of steps leading to Eq. (31) to recast the Hamiltonian of Eq. (33) in a fermionic form. The end result is just the original multichannel Kondo Hamiltonian of Eq. (19) with the following set of renormalized parameters:

$$J_z \to J_z' = \frac{4}{\pi\rho} \tan\left( \frac{\pi}{k} - \delta_z \right), \tag{34}$$

$$h \to -h, \tag{35}$$

$$g_i \to 2g_e - g_i. \tag{36}$$

For zero magnetic field, this establishes the mapping of Eq. (1), including the restriction to values of $J_z$ where the right-hand side of Eq. (1) does not exceed $\pi/2$. The latter condition is just a restatement of the requirement $|\delta_z'| \leq \pi/2$. We now analyze in detail the ramifications of this restriction as a function of the number of channels $k$.

For $k=1$ (single-channel case), $\delta_z'$ exceeds $\pi/2$ for all $-\infty < J_z < \infty$. Thus, the mapping of Eq. (1) does not apply to the single-channel Kondo effect, in accordance with known results. For $k=2$ (two-channel case), the required condition is met for all $J_z \geq 0$, mapping weak to strong coupling and vice versa [see Eq. (2)]. Hence, the mapping of Eq. (1) can be viewed as an anisotropic variant[20] of the strong-to-weak-coupling duality of Noziéres and Blandin.[25]

The most interesting case occurs for $k>2$ when Eq. (1) extends to all $J_z \geq J_{\min}$, with

$$J_{\min} = -\frac{4}{\pi\rho} \tan\left( \frac{\pi}{2} - \frac{\pi}{k} \right) < 0. \tag{37}$$

In particular, the range $J_z > J_z^*$ with

$$J_z^* = \frac{4}{\pi\rho} \tan\left( \frac{\pi}{k} \right) > 0 \tag{38}$$

is mapped onto the negative-coupling regime $J_{\min} \leq J_z' < 0$ and vice versa. Thus, the Kosterlitz-Thouless line separating the antiferromagnetic and ferromagnetic domains is duplicated from $J_z = -|J_\perp|$ to $J_z = J_z^* + C_k |J_\perp|$, with

$$C_k = \frac{1}{1+\tan^2(\pi/k)} = \frac{1}{1+(\pi\rho J_z^*/4)^2}. \quad (39)$$

Here, we have assumed $\rho|J_z - J_z^*|, \rho|J_\perp| \ll 1$ in order for the weak-coupling form of the Kosterlitz-Thouless line to apply.

The resulting phase diagram for $k>2$ is plotted in Fig. 1(a). For $J_z > J_z^* + C_k|J_\perp|$, the multichannel Kondo Hamiltonian flows to a line of stable ferromagneticlike fixed points, restricting the basin of attraction of the overscreened non-Fermi-liquid fixed point to the domain $-|J_\perp| < J_z < J_z^* + C_k|J_\perp|$. The antiferromagnetic regime therefore divides into two vastly different regions: an overscreened non-Fermi-liquid domain and a ferromagneticlike domain. Such behavior has no parallel for $k \leqslant 2$. Note that the same phase diagram as the one depicted in Fig. 1(a) also emerges from the renormalization-group equations derived by Ye using the equivalent Anderson-Yuval approach.[21] However, the newly found line of stable ferromagneticlike fixed points has eluded Ye.

## IV. STRONG-COUPLING EXPANSION FOR $s=1/2$

A potential concern with the resulting phase diagram for $s=1/2$ and $k>2$ has to do with the validity of the bosonization approach used. Since $J_z^*$ exceeds the bandwidth $D$ for intermediate values of $k$, one might wonder to what extent is bosonization (or the Anderson-Yuval approach for that matter) justified for such strong coupling. In fact, the very usage of the continuum-limit Hamiltonian of Eq. (19) with its unbounded linear dispersion can be called into question. Could it be that $J_z^* \to \infty$ when the conduction electrons are placed on a lattice?

Notwithstanding the observation that $J_z^*$ for $k \gg 1$ is pushed to weak coupling, to firmly establish the phase diagram of Fig. 1(a), one must show that the new line of stable ferromagneticlike fixed points extends to proper lattice models for the underlying conduction bands. This is the objective of the following analysis, which focuses on the limit of a large longitudinal coupling, $J_z \gg D, |J_\perp|$.

As a generic lattice model for the conduction bands, we consider a spin-$\frac{1}{2}$ impurity moment coupled to the open end of a semi-infinite tight-binding chain with $k$ identical conduction-electron species. The corresponding Hamiltonian, depicted schematically in Fig. 2(a), is given by

$$\mathcal{H} = \sum_{j=0}^{\infty}\sum_{n=1}^{k}\sum_{\sigma=\uparrow,\downarrow}[\epsilon_j f_{jn\sigma}^\dagger f_{jn\sigma} + t_j\{f_{(j+1)n\sigma}^\dagger f_{jn\sigma} + \text{H.c.}\}]$$
$$+ \frac{J_\perp}{2}\sum_{n=1}^{k}[f_{0n\downarrow}^\dagger f_{0n\uparrow} S^+ + \text{H.c.}] + \frac{J_z}{2}\sum_{n=1}^{k} S_z[f_{0n\uparrow}^\dagger f_{0n\uparrow} - f_{0n\downarrow}^\dagger f_{0n\downarrow}]$$
$$- g_i h S_z - \frac{g_e h}{2}\sum_{j=0}^{\infty}\sum_{n=1}^{k}[f_{jn\uparrow}^\dagger f_{jn\uparrow} - f_{jn\downarrow}^\dagger f_{jn\downarrow}], \quad (40)$$

where $\epsilon_j$ and $t_j$, respectively, are the on-site energies and the hopping matrix elements along the chain. Any lattice model with identical noninteracting bands can be cast in the form of Eq. (40) using a Wilson-type construction.[19] Different lattice models are distinguished by the tight-binding parameters $\epsilon_j$ and $t_j$, the largest of which determines the bandwidth $D$. For example, particle-hole symmetry demands that $\epsilon_j=0$ for all sites along the chain. In the following, we assume a large longitudinal coupling, $J_z \gg D, |J_\perp|$, and expand in powers of $1/J_z$ to derive an effective Hamiltonian at energies far below $J_z$.

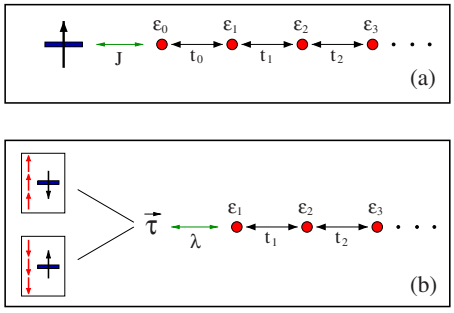


FIG. 2. (Color online) (a) Schematic sketch of the semi-infinite tight-binding chain of Eq. (40) with the impurity spin coupled to its open end. Here, $J$ represents the anisotropic spin-exchange interaction $J_z \gg D, |J_\perp|$. (b) The effective Hamiltonian obtained for $J_z \gg k_B T$. In order to satisfy the large longitudinal exchange coupling $J_z$, the impurity spin combines with the local conduction-electron degrees of freedom at site $j=0$ to form a composite isospin-$\frac{1}{2}$ degree of freedom $\vec{\tau}$ (depicted here for the case $k=3$). The isospin $\vec{\tau}$ couples weakly to the conduction electrons at site $j=1$ through the "exchange" term $\lambda=(\lambda_z,\lambda_\perp)$, whose form varies with the number of channels $k$ as described in the text.

For $k_B T \ll J_z$, the fermionic degrees of freedom at site zero tightly bind to the impurity so as to minimize the $J_z$ interaction term. There are two degenerate ground states of the $J_z$ interaction term, corresponding to the total spin projections $S_{\text{total}}^z = \pm(k-1)/2$:

$$|+\rangle = \prod_{n=1}^{k} f_{0n\uparrow}^\dagger |S_z = \downarrow\rangle, \quad |-\rangle = \prod_{n=1}^{k} f_{0n\downarrow}^\dagger |S_z = \uparrow\rangle. \quad (41)$$

All excited eigenstates of the $J_z$ term are thermally inaccessible, being removed in energy by integer multiples of $J_z/4$. Defining a new isospin operator $\vec{\tau}$ according to

$$\tau_z = \frac{1}{2}\sum_{p=\pm} p|p\rangle\langle p|, \quad \tau^\pm = |\pm\rangle\langle\mp| \quad (42)$$

[compare with Eqs. (13) and (14) and Eqs. (16) and (17) in the weak-coupling limit], the effective low-energy Hamiltonian takes the form $\mathcal{H}_{\text{chain}} + \mathcal{H}_{\text{mag}} + \mathcal{H}_{\text{int}}$, where $\mathcal{H}_{\text{chain}}$ is the tight-binding Hamiltonian of the truncated chain with site $j=0$ removed, $\mathcal{H}_{\text{mag}}$ is the magnetic-field term

$$\mathcal{H}_{\text{mag}} = -g_\tau h \tau_z - \frac{g_e h}{2}\sum_{j=1}^{\infty}\sum_{n=1}^{k}[f_{jn\uparrow}^\dagger f_{jn\uparrow} - f_{jn\downarrow}^\dagger f_{jn\downarrow}] \quad (43)$$

with $g_\tau = k g_e - g_i$, and $\mathcal{H}_{\text{int}}$ contains all finite-order corrections in either $1/J_z$ or $J_\perp$ (or both). The resulting Hamiltonian is sketched schematically in Fig. 2(b) for $k=3$.

The explicit form of the Hamiltonian term $\mathcal{H}_{\text{int}}$ depends on the number of conduction-electron channels $k$. For $k=1$ and up to linear order in $1/J_z$, it takes the form

$$\mathcal{H}_{\rm int} = J_\perp \tau_x + \frac{\lambda_z}{2}\tau_z[f^\dagger_{1\uparrow}f_{1\uparrow} - f^\dagger_{1\downarrow}f_{1\downarrow}], \tag{44}$$

where $\lambda_z$ equals

$$\lambda_z = \frac{4t_0^2}{J_z} \ll D. \tag{45}$$

Here, we have set $f^\dagger_{1n\sigma} \to f^\dagger_{1\sigma}$, omitting the redundant channel index $n$ from within $f^\dagger_{1n\sigma}$. Since the $\lambda_z$ term is exactly marginal, the low-temperature physics is governed for $h=0$ by the spin-flip term $J_\perp$, which favors the spin-singlet state $\frac{1}{\sqrt{2}}[|+\rangle - |-\rangle]$ over the spin-triplet state $\frac{1}{\sqrt{2}}[|+\rangle + |-\rangle]$ for $J_\perp > 0$. In this manner, one recovers the characteristic spin singlet of the single-channel Kondo effect, restoring SU(2) spin symmetry as $T \to 0$. A local magnetic field breaks the emerging SU(2) spin symmetry, as it physically should, by introducing weak spin-dependent scattering at the open end of the truncated chain.

The situation is somewhat different for $k=2$. In this case, $\mathcal{H}_{\rm int}$ acquires the form

$$\mathcal{H}_{\rm int} = \frac{\lambda_z}{2}\tau_z \sum_{n=1}^{2}[f^\dagger_{1n\uparrow}f_{1n\uparrow} - f^\dagger_{1n\downarrow}f_{1n\downarrow}] + \lambda_\perp \sum_{n=1}^{2}[f^\dagger_{1n\uparrow}f_{1n\downarrow}\tau^- + \text{H.c.}], \tag{46}$$

where $\lambda_z$ is still given to linear order in $1/J_z$ by Eq. (45) and $\lambda_\perp$ scales as

$$\lambda_\perp \sim \frac{J_\perp t_0^2}{J_z^2}. \tag{47}$$

Here, we have omitted higher order interaction terms within $\mathcal{H}_{\rm int}$ and restricted attention to particle-hole symmetry. Away from particle-hole symmetry, an additional potential-scattering term of the form $\Delta\epsilon_1 \Sigma_n f^\dagger_{1n\sigma}f_{1n\sigma}$ is generated at second order in $1/J_z$.

Equation (46) has the same exact form as the original spin-exchange interaction in Eq. (40), modulo three modifications. (i) The coupling constants $J_z$ and $J_\perp$ have been pushed to weak coupling. (ii) The site $j=0$ has been replaced with $j=1$. (iii) The physical content of the local moment $\vec{\tau}$ has changed. Importantly, since $D \gg \lambda_z \gg |\lambda_\perp|$, one lies within the confines of the antiferromagnetic domain, rendering $\mathcal{H}_{\rm int}$ a relevant perturbation. Hence, in accordance with the bosonization treatment of Sec. III, the strong-coupling limit $J_z \gg D$ maps onto weak coupling, extending the duality of Noziéres and Blandin[25] to large spin-exchange anisotropy. Indeed, since $t_0 \sim 1/\rho$ for conventional lattice models, then $\lambda_z$ of Eq. (45) is comparable in magnitude to $J_z'$ of Eq. (2). The main difference as compared to bosonization pertains to the transverse coupling $J_\perp$, which renormalizes to $\lambda_\perp \propto 1/J_z^2$ in the strong-coupling expansion but is left unchanged within bosonization. Excluding this rather minor discrepancy, the two approaches are in close agreement with one another.

A crucial difference for $k>2$ has to do with the dynamic components of $\mathcal{H}_{\rm int}$, responsible for flipping the isospin $\vec{\tau}$. To see this, we note that the states $|\pm\rangle$ have the spin projections $S^z_{\rm total} = \pm(k-1)/2$, which differ by $k-1$. Since the Hamiltonian of Eq. (40) preserves the overall spin projection of the entire system, the flipping of $\tau_z$ in either direction must be accompanied by an opposite spin flip of $k-1$ electrons along the truncated chain. Hence, the leading dynamic term in $\mathcal{H}_{\rm int}$ can only show up at order $(1/J_z)^{2(k-1)}$, taking the form

$$\lambda_\perp \left[ \tau^- \sum_{m=1}^{k} \prod_{n\neq m} f^\dagger_{1n\uparrow}f_{1n\downarrow} + \text{H.c.} \right], \tag{48}$$

with

$$\lambda_\perp \sim J_\perp \left(\frac{t_0}{J_z}\right)^{2(k-1)}. \tag{49}$$

In contrast to the dynamic part, the leading static component of $\mathcal{H}_{\rm int}$ remains given by the $\lambda_z$ term of Eq. (46), except for the summation over $n$ which now runs over all $k$ channels. To linear order in $1/J_z$, the coupling $\lambda_z$ is independent of $k$ and is given by Eq. (45). Once again, an additional potential-scattering term is generated at order $(1/J_z)^2$ away from particle-hole symmetry.

Since the $\lambda_\perp$ term of Eq. (48) involves the creation and annihilation of $k-1$ electrons at the open end of the truncated chain, it has the scaling dimension $\Delta_\perp = k-1$ with respect to the "free" $J_z \to \infty$ Hamiltonian. Hence, this term is irrelevant for $k>2$. The same holds true of all higher order dynamical terms generated, as these likewise contain at least $k-1$ creation and $k-1$ annihilation operators for electrons localized along the truncated chain. Similar to the case $s>1/2$ and $|J_z| > |J_\perp|$ at weak coupling (see Sec. II), the resulting fixed-point Hamiltonian corresponds for $h=0$ to a finite longitudinal coupling $\lambda_z$ but zero $\lambda_\perp$, in perfect agreement with the predictions of bosonization. In fact, an identical scaling dimension $\Delta_\perp \to k-1$ is obtained in the Anderson-Yuval approach for $\rho J_z \gg 1$,[26] reinforcing the qualitative agreement between these vastly different approaches. Thus, a line of stable ferromagneticlike fixed points is seen to exist for any lattice model with sufficiently large $J_z > 0$, as predicted by bosonization.

Evidently, the strong-coupling expansion confirms the results of bosonization for all three cases: $k=1$, $k=2$, and $k>2$. Moreover, it provides a very transparent physical picture for the source of distinction between the three cases. It all boils down to the nature of the local spin configurations selected by a sufficiently large $J_z > 0$. We therefore conclude that Fig. 1(a) correctly describes the phase diagram of the spin-$\frac{1}{2}$ multichannel Kondo model with $k>2$ conduction-electron channels.

## V. STRONG-COUPLING EXPANSION FOR ARBITRARY SPIN $s$

Our discussion in the previous two sections was confined to a spin-$\frac{1}{2}$ impurity. An appealing feature of the strong-coupling expansion in $1/J_z$ is that it can easily be generalized to arbitrary spin $s$. This is the goal of the present section.

The basic considerations for arbitrary $s>1/2$ are quite similar to those for $s=1/2$. As before, the $J_z$ interaction term possesses two degenerate ground states, whom we label by $|\pm\rangle$. For $k \geqslant 2s$, these states are given by

$$|+\rangle = \prod_{n=1}^{k} f_{0n\uparrow}^{\dagger}|S_z = -s\rangle, \quad |-\rangle = \prod_{n=1}^{k} f_{0n\downarrow}^{\dagger}|S_z = s\rangle, \quad (50)$$

while for $k<2s$, they take the form

$$|+\rangle = \prod_{n=1}^{k} f_{0n\downarrow}^{\dagger}|S_z = s\rangle, \quad |-\rangle = \prod_{n=1}^{k} f_{0n\uparrow}^{\dagger}|S_z = -s\rangle. \quad (51)$$

With this convention, $|\pm\rangle$ have the total spin projections $S^z_{\text{total}} = \pm|k/2-s|$. Defining an isospin $\vec{\tau}$ according to Eq. (42), the effective low-energy Hamiltonian is written as $\mathcal{H}_{\text{chain}}+\mathcal{H}_{\text{mag}}+\mathcal{H}_{\text{int}}$, where $\mathcal{H}_{\text{chain}}$ is the tight-binding Hamiltonian of the truncated chain with site $j=0$ removed, $\mathcal{H}_{\text{mag}}$ is the magnetic-field term of Eq. (43), and $\mathcal{H}_{\text{int}}$ contains all finite-order corrections in either $1/J_z$ or $J_\perp$ (or both). The sole modification to $\mathcal{H}_{\text{mag}}$ as compared to the spin-$\frac{1}{2}$ case is in the form of the effective $g$ factor $g_\tau$, which generalizes from $g_e k - g_i$ when $s=1/2$ to $\pm(g_e k - 2s g_i)$ for arbitrary $s$. Here, the plus (minus) sign corresponds to $k \geqslant 2s$ ($k<2s$).

Similar to the case $s=1/2$, the delicate interplay between $k$ and $s$ enters through the Hamiltonian term $\mathcal{H}_{\text{int}}$. Let us separate the discussion of the dynamic and static components of $\mathcal{H}_{\text{int}}$, as these depend differently on $s$ and $k$. The leading static component of $\mathcal{H}_{\text{int}}$ remains given by the $\lambda_z$ term of Eq. (46), except for the summation over $n$ which now runs over all $k$ conduction-electron channels. The coupling $\lambda_z$ does depend on $k-2s$, however, only through its overall sign. For $k \geqslant 2s$, it is given to order $1/J_z$ by Eq. (45), corresponding to an antiferromagnetic interaction. For $k<2s$, it acquires an additional minus sign, corresponding to a ferromagnetic interaction. Apart from its overall sign, the leading static component of $\mathcal{H}_{\text{int}}$ is independent of $s$.

Moving on to the dynamic part of $\mathcal{H}_{\text{int}}$, its leading-order component displays a more elaborate dependence on $k$ and $s$. As noted above, the total spin projections for the states $|+\rangle$ and $|-\rangle$ differ by $|k-2s|$. Consequently, the flipping of $\tau_z$ in either direction must be accompanied by an opposite spin flip of $|k-2s|$ electrons along the truncated chain. Otherwise, the total spin projection of the system is not conserved. This consideration dictates the following form for the leading dynamical term:

$$\lambda_\perp[\tau^- \hat{O}^+_{k,s} + \tau^+ \hat{O}^-_{k,s}], \quad (52)$$

where $\hat{O}^+_{k,s} = (\hat{O}^-_{k,s})^\dagger$ is a channel-symmetric operator that creates $|k-2s|$ spin-up electrons and annihilates $|k-2s|$ spin-down electrons at, or close as possible to, the open end of the truncated chain.

The operator $\hat{O}^+_{k,s}$ is generally too complicated to write down. It greatly simplifies in two cases: (i) for $k=2s$, when $\hat{O}^+_{k,s}$ reduces to the unity operator, and (ii) for $s=1/2$ and $k>1$, when $\hat{O}^+_{k,s}$ is given by Eq. (48). As for the coupling $\lambda_\perp$, it scales differently for $k \geqslant s$ and $k<s$. For $k \geqslant s$, $\lambda_\perp$ scales as

$$\lambda_\perp \sim J_\perp \left(\frac{J_\perp}{J_z}\right)^{2s-1} \left(\frac{t_0}{J_z}\right)^{2|k-2s|}. \quad (53)$$

For $k<s$, it scales with a higher power of $1/J_z$, as electrons farther into the chain must participate in the flipping of $\tau_z$. With the possible exception of $k=2s$, the transverse coupling $|\lambda_\perp|$ is parametrically smaller than $|\lambda_z|$, a fact that will have important implications later on.

As a function of $s$ and $k$, $\lambda_\perp$ has the scaling dimension $\Delta_\perp = |k-2s|$ with respect to the "free" $J_z \to \infty$ Hamiltonian. For $h=0$, this yields the following classification of the low-energy physics.

(*i*) $s=k/2$. In this exactly screened case, $\lambda_\perp$ acts as a local transverse magnetic field, lifting the twofold degeneracy of $|\pm\rangle$. Although the local state favored by $\lambda_\perp$ is generally not an SU(2) spin singlet, the low-energy physics is identical to that obtained for isotropic spin exchange, as can be seen from the boundary condition imposed on the truncated chain. In particular, a local Fermi liquid progressively forms below the Kondo temperature $T_K \sim \lambda_\perp$.

(*ii*) $s=k/2-1/2$. In this overscreened case, the Hamiltonian term $\mathcal{H}_{\text{int}}$ has the same exact form as Eq. (46), except for the summation over $n$ which now runs over all $k$ conduction-electron channels. Hence, the system is described by a weakly coupled $k$-channel Kondo Hamiltonian with $\lambda_z \gg |\lambda_\perp| > 0$. The effect of a large spin-exchange anisotropy in the original Hamiltonian is therefore to reduce the effective impurity moment from $s$ to $1/2$. Based on the perturbative RG analysis of Sec. II, the resulting Hamiltonian flows to the overscreened fixed point of the $k$-channel, spin-$\frac{1}{2}$ Kondo Hamiltonian, which is equivalent in turn to that of the $k$-channel Kondo model with $s=k/2-1/2$. As in the exactly screened case discussed above, a large spin-exchange anisotropy $J_z \gg D, |J_\perp|$ does not affect the nature of the low-energy fixed point for $s=k/2-1/2$.

(*iii*) $s=k/2+1/2$. Similar to the previous case, the system is described by a weakly coupled $k$-channel Kondo Hamiltonian with $s \to 1/2$. However, the effective coupling is now ferromagnetic: $-\lambda_z \gg |\lambda_\perp| > 0$. Consequently, the flow is to a line of stable ferromagneticlike fixed points with a finite $\lambda_z$ but zero $\lambda_\perp$. The resulting low-energy physics is that of a singular Fermi liquid[13] plus a residual isospin $\vec{\tau}$. It differs from that of an isotropic spin-exchange interaction only in the residual $\lambda_z$ term, which is marginal in nature. The effect of a large spin-exchange anisotropy on this underscreened case is therefore to introduce an additional marginal term.

(*iv*) $|k-2s|>1$. In this effectively underscreened case, the scaling dimension $\Delta_\perp$ exceeds 1. Hence, $\lambda_\perp$ is irrelevant, as are all higher order dynamical terms generated within $\mathcal{H}_{\text{int}}$. The system thus flows to a line of stable ferromagneticlike fixed points, characterized by a finite $\lambda_z$ but zero $\lambda_\perp$. The low-energy physics is again that of a (potentially singular) Fermi liquid with a residual isospin $\vec{\tau}$. For $s<k/2-1/2$, this differs markedly from the overscreened fixed point of the isotropic model. Also for $s>k/2+1/2$ does this differ from the underscreened fixed point of the isotropic model, as the residual degeneracy is 2 instead of $2s-k+1>2$. Importantly, the resulting low-energy physics is insensitive to the sign of $k-2s$, in stark contrast to the isotropic case. A large spin-exchange anisotropy $J_z \gg D, |J_\perp|$ therefore alters the fixed-point structure for all $|k-2s|>1$ as compared to the isotropic case.

The phase diagram of the multichannel Kondo Hamiltonian with $J_z \gg |J_\perp|, D$ is summarized in Fig. 3 as a function of $k$ and $s$. Excluding the exactly screened line $2s=k$ and the

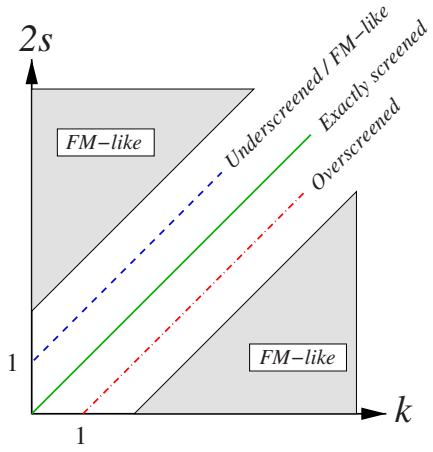


FIG. 3. (Color online) Phase diagram of the multichannel Kondo model with $J_z \gg |J_\perp|, D$ as a function of $k$ and $s$. For $2s=k$ and $2s=k-1$, the low-energy physics is unaffected by such a large spin-exchange anisotropy. The fixed point remains that of an exactly screened $(2s=k)$ or an overscreened $(2s=k-1)$ Kondo effect. For $|k-2s|>1$, the low-energy physics is substantially altered by the large spin-exchange anisotropy. The system flows to a line of stable ferromagneticlike fixed points with a residual isospin-$\frac{1}{2}$ local moment. This should be contrasted with the isotropic case, where the flow is either to an overscreened fixed point (when $k>2s+1$) or to an underscreened fixed point with a residual local moment of size $s-k/2>1/2$ (when $2s>k+1$). For $2s=k+1$, a large spin-exchange anisotropy has only a marginal effect on the low-energy physics. The system still flows to a line of stable ferromagneticlike fixed points as in the case where $|k-2s|>1$; however, the resulting fixed points are distinguished from the isotropic underscreened one only by the marginal operator $\lambda_z$ (see text for details).

overscreened line $2s=k-1$, the model flows to a line of stable ferromagneticlike fixed points with a residual isospin-$\frac{1}{2}$ local moment for all $k$ and $s$. For $2s=k+1$, the ferromagneticlike fixed points and the isotropic underscreened fixed point are equivalent. They differ only by the marginal term $\lambda_z$. For $2s>k+1$, these fixed points are distinctly different, possessing different residual degeneracies.

## VI. NUMERICAL RENORMALIZATION-GROUP STUDY OF $s=1/2$, $k=3$

Although the strong-coupling expansion unequivocally confirms the existence of a line of stable ferromagneticlike fixed points for large $J_z$ and $|k-2s|>1$, it cannot access the entire phase diagram of the anisotropic multichannel Kondo Hamiltonian. In particular, the second Kosterlitz-Thouless line predicted by bosonization for $s=1/2$ and $k>2$ [see Fig. 1(a)] lies beyond the scope of this approach. In this section, we use Wilson's numerical renormalization-group (NRG) method[19] to conduct a systematic study of the phase diagram of the anisotropic multichannel Kondo Hamiltonian with $s=1/2$ and $k=3$.

In conventional formulations of the NRG,[19] one considers a particular choice for the tight-binding parameters of Eq. (40), given by $\epsilon_j=0$ and $t_j=D_\Lambda \Lambda^{-j/2}\xi_j$, with

$$D_\Lambda = \frac{D}{2}(1+\Lambda^{-1}), \tag{54}$$

$$\xi_j = \frac{1-\Lambda^{-(j+1)}}{\sqrt{(1-\Lambda^{-(2j+1)})(1-\Lambda^{-(2j+3)})}}. \tag{55}$$

Here, $\Lambda>1$ is a discretization parameter. For $\Lambda \to 1^+$, the resulting model describes an impurity spin locally coupled to $k$ identical conduction bands with a symmetric box density of states $\rho(E)=(1/2D)\theta(D-|E|)$. For $\Lambda>1$, the model represents an impurity spin coupled to a logarithmically discretized version of the same bands.[19]

The first step in the NRG approach is to recast the Hamiltonian $\mathcal{H}$ as the limit of a sequence of dimensionless Hamiltonians $\mathcal{H}_N$:

$$\mathcal{H} = \lim_{N\to\infty}\{D_\Lambda \Lambda^{-(N-1)/2}\mathcal{H}_N\}, \tag{56}$$

with

$$\mathcal{H}_N = \Lambda^{(N-1)/2}\Bigg[\frac{J_\perp}{2D_\Lambda}\sum_{n=1}^{k}(f_{0n\downarrow}^\dagger f_{0n\uparrow}S^+ + \text{H.c.}) + \frac{J_z}{2D_\Lambda}\sum_{n=1}^{k}S_z(f_{0n\uparrow}^\dagger f_{0n\uparrow} - f_{0n\downarrow}^\dagger f_{0n\downarrow}) + \sum_{j=0}^{N-1}\sum_{n=1}^{k}\sum_{\sigma=\uparrow,\downarrow}\Lambda^{-j/2}\xi_j\{f_{(j+1)n\sigma}^\dagger f_{jn\sigma} + \text{H.c.}\}\Bigg]. \tag{57}$$

The finite-size Hamiltonians $\mathcal{H}_N$ are then diagonalized iteratively using the NRG transformation

$$\mathcal{H}_{N+1} = \sqrt{\Lambda}\mathcal{H}_N + \sum_{n=1}^{k}\sum_{\sigma=\uparrow,\downarrow}\xi_N\{f_{(N+1)n\sigma}^\dagger f_{Nn\sigma} + \text{H.c.}\}. \tag{58}$$

Here, the prefactor $\Lambda^{(N-1)/2}$ in Eq. (57) guarantees that the low-energy excitations of $\mathcal{H}_N$ are of order one for all $N$. The approach to a fixed-point Hamiltonian is signaled by a limit cycle of the NRG transformation, with $\mathcal{H}_{N+2}$ and $\mathcal{H}_N$ sharing the same low-energy spectrum.

In practice, it is impossible to keep track of the exponential increase in the size of the Hilbert space as a function of the chain length $N$. Hence, only the lowest $N_s$ eigenstates of $\mathcal{H}_N$ are retained at the conclusion of each iteration.[27] The retained states are used in turn to construct the eigenstates of $\mathcal{H}_{N+1}$. The truncation error involved can be systematically controlled by varying $N_s$. However, since the size of the Hilbert space increases by a factor of $2^{2k}$ with each additional iteration, only a moderately small number of conduction-electron channels can be treated reliably using present-day computers, typically no more than 3 or 4. In the following, we focus on $k=3$ and $s=1/2$, which is the simplest variant of the multichannel Kondo Hamiltonian that is both amendable to the NRG and predicted to display the phase diagram of Fig. 1(a).

To cope with the large computational effort involved in exploring the phase diagram of the three-channel Kondo model with spin-exchange anisotropy, we used rather large values of $\Lambda$ (either $\Lambda=3$ or $\Lambda=5$) and applied an alternative

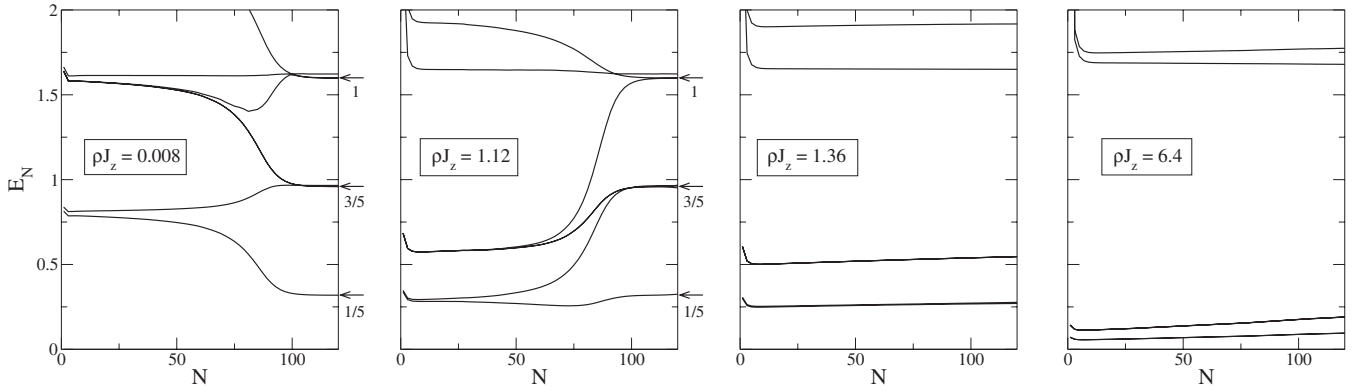


FIG. 4. NRG level flow (odd iterations) for $s=1/2$, $k=3$, $\rho J_\perp=0.008$, and increasing values of $\rho J_z$. Here, $\Lambda$ equals 3. For $\rho J_z<\rho J_z^c \approx 1.26$ (left two panels), the system flows to the non-Fermi-liquid fixed point of the three-channel Kondo effect irrespective of $J_z$. There is excellent agreement with the finite-size spectrum of the three-channel Kondo effect obtained from conformal field theory, whose energy levels (in units of the fundamental level spacing) are indicated by arrows. For $J_z>J_z^c$ (right two panels), the finite-size spectrum remains Fermi-liquid-like down to minuscule energies, without crossing over to the non-Fermi-liquid fixed point of the three-channel Kondo effect. The persisting drift of NRG levels for $J_z>J_z^c$ appears to be driven by some weak numerical instability. A similar drift of levels occurred for $-J_z \gg J_\perp>0$ (ferromagnetic coupling).

truncation scheme to the one customarily used. Since each of the NRG Hamiltonians $\mathcal{H}_N$ is block diagonal in the conserved quantum numbers,[28] the computational time is mostly governed by the largest block to be diagonalized. Thus, instead of retaining a fixed number of eigenstates of $\mathcal{H}_N$ at the conclusion of each iteration, we adjusted the threshold energy for truncation so that the largest block retained did not exceed $N_{\text{block}}$ states.[27] For $\Lambda=3$, we used $N_{\text{block}}=100$, while for $\Lambda=5$, we set $N_{\text{block}}=80$. This strategy gave rise to variations in the number of states retained at the conclusion of each iteration. Typically, between 3000 and 4000 states were kept. However, in some extreme cases, down to 2500 and up to 5500 states were retained. We have verified that the threshold energies selected in this way were sufficiently high so as not to affect the accuracy of the calculations.

Figure 4 depicts the finite-size spectra obtained for $\rho J_\perp=0.008$ and different values of $\rho J_z>0$. Here, $\Lambda=3$ was used. Up to a critical coupling $\rho J_z^c \approx 1.26$, the system always flows to the non-Fermi-liquid fixed point of the three-channel Kondo effect. Indeed, the fixed-point spectrum is independent of $J_z<J_z^c$ and is identical to the one obtained for isotropic spin exchange (leftmost panel). There is excellent agreement with the finite-size spectrum of the three-channel Kondo effect predicted by conformal field theory,[29] whose energy levels are marked by arrows in Fig. 4. Note the slight splitting of NRG levels near the dimensionless energy 1.6, which is a $\Lambda$-dependent feature. It is reduced in size upon decreasing $\Lambda$ and should disappear for $\Lambda \to 1^+$.

A different picture is recovered for $J_z>J_z^c$. (i) As demonstrated in Fig. 4 for $\rho J_z=1.36$ and $\rho J_z=6.4$, the finite-size spectrum remains Fermi-liquid-like down to the lowest energies reached ($E \sim 10^{-120} D$ in some extreme runs), without crossing over to the overscreened fixed point of the three-channel Kondo effect. (ii) The finite-size spectrum varies continuously with $J_z>J_z^c$, suggesting the flow to a line of fixed points connected by a marginal operator. (iii) For $J_z \gg J_z^c$, the quantum numbers and degeneracies of the NRG levels are in excellent agreement with those anticipated based on the strong-coupling analysis of Sec. IV. (iv) The NRG level flow confirms that channel asymmetry is a marginal perturbation for $J_z>J_z^c$ (not shown), in stark contrast to the regime $J_z<J_z^c$. These features are all consistent with the flow to a line of stable ferromagneticlike fixed points as predicted by bosonization.

We do note, however, a persisting drift of the NRG levels for $J_z>J_z^c$. A similar drift of levels occurred for $-J_z \gg |J_\perp| >0$ (ferromagnetic coupling) and is presumably driven by some weak numerical instability. While we cannot entirely rule out an eventual crossover to the non-Fermi-liquid fixed point of the three-channel Kondo effect at yet some lower temperature, we find this scenario highly unlikely given the extremely low energy scales reached and the rapid change of behavior as $J_z$ is swept across $J_z^c$. We therefore identify $J_z^c$ with the phase boundary between the antiferromagnetic and the new ferromagneticlike domain predicted by bosonization.

Adopting this interpretation, we turn to explore the dependence of $J_z^c$ on $J_\perp$. The resulting phase diagram is plotted in Fig. 5 for $\Lambda=5$. While points on the solid line have all converged to the non-Fermi-liquid fixed point of the three-channel Kondo effect, points on the dashed line showed no such tendency up to $N=120$ NRG iterations (corresponding to $E \sim 10^{-42} D$). We therefore estimate the phase boundary between the antiferromagnetic and the ferromagneticlike domains to lie in between the solid and dashed lines. In contrast to the solid line, which definitely lies on the antiferromagnetic side of the transition, one cannot guarantee that all points on the dashed line lie on the ferromagneticlike side. We have confirmed, however, that the phase diagram of Fig. 5 is practically unchanged upon going to $N=180$ iterations. We further stress that the exact position of the phase boundary is generally $\Lambda$ dependent, although the dependence on $\Lambda$ is evidently weak. For example, the position of the phase boundary varied by no more than just a few percent in going to $\Lambda=3$. We anticipate a similar proximity of the $\Lambda \to 1^+$ phase boundary.

The above results are clearly in good qualitative agreement with the bosonization treatment of Sec. III. We now

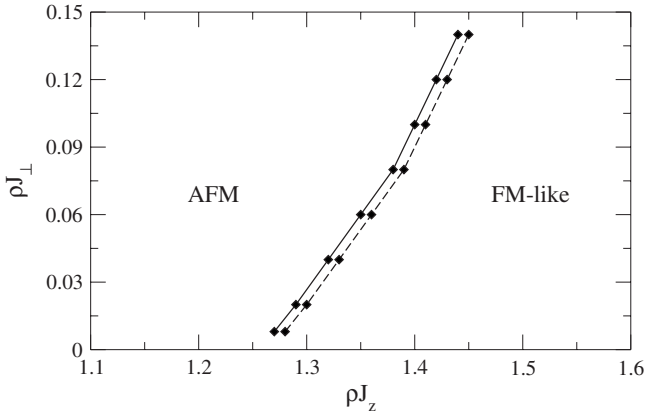


FIG. 5. NRG phase boundary between the antiferromagnetic domain and the new ferromagneticlike domain for $s=1/2$, $k=3$, and $\Lambda=5$. Points on the solid line all converged to the non-Fermi-liquid fixed point of the three-channel Kondo effect. Points on the dashed line showed no such tendency up to $N=120$ NRG iterations, corresponding to $E\sim 10^{-42}D$. We estimate the phase boundary between the two domains to lie in between the solid and dashed lines.

turn to a more quantitative comparison. Setting $k=3$ in Eq. (38), the critical coupling $J_z^*$ predicted by bosonization is equal to $\rho J_z^*=4\sqrt{3}/\pi\approx 2.2$. Based on the NRG results for $\Lambda=3$ and $\Lambda=5$, we estimate the location of the critical coupling for a symmetric box density of states (i.e., for $\Lambda\to 1^+$) to lie in the vicinity of $\rho J_z^*\sim 1.2-1.3$. Thus, the bosonization and NRG results fall within a factor of 2 from one another. Considering that $J_z^*$ lies well beyond the strict range of validity of bosonization, we find this degree of agreement to be quite remarkable. As for the shape of the phase boundary, it was predicted in Sec. III to have the linear form $J_z=J_z^*+C_k|J_\perp|$, where $0<C_k<1$ is given by Eq. (39). As seen in Fig. 5, the NRG phase boundary for $\Lambda=5$ is well described by a linear curve, at least up to $\rho J_\perp\approx 0.08$. The corresponding slope $C_{\rm NRG}\approx 0.67$ is indeed less than 1 but is nearly threefold larger than the bosonization result, $C_{k=3}=0.25$. This discrepancy can be largely overcome by plugging the NRG value for $\rho J_z^*$ into the right-hand side of Eq. (39), which yields $C\approx 0.5$.

## VII. DISCUSSION AND SUMMARY

The multichannel Kondo Hamiltonian is an important paradigm in correlated electron systems, with possible applications to varied systems. Depending on the size of the impurity spin $s$ and the number of independent conduction-electron channels $k$, it can display either local Fermi-liquid, singular Fermi-liquid, or non-Fermi-liquid behaviors. Although the isotropic model is by now well understood, we have shown in this paper that an *XXZ* spin-exchange anisotropy has a far more elaborate effect on its low-energy physics than previously appreciated. A detailed account of our results is presented in Fig. 1. Below, we summarize our main findings and speculate about certain coupling regimes not covered by our treatment.

We begin with a spin-$\frac{1}{2}$ impurity and with $k>2$ conduction-electron channels. From conformal field theory it is known that the overscreened non-Fermi-liquid fixed point of the corresponding Kondo model is stable against a weak spin-exchange anisotropy.[16] However, the non-Fermi-liquid fixed point is no longer approached when $J_z\gg|J_\perp|>0$ is sufficiently large. In the latter regime, the system flows to a line of stable ferromagneticlike fixed points with a residual isospin-$\frac{1}{2}$ local moment. The phase diagram of the model thus consists of three distinct domains: the conventional ferromagnetic and antiferromagnetic (i.e., non-Fermi-liquid) domains plus a third ferromagneticlike domain located deep inside the antiferromagnetic regime. The new ferromagneticlike domain extends above a critical longitudinal coupling $J_z^*$, whose magnitude depends on $k$. While $J_z^*$ exceeds the bandwidth for intermediate values of $k$, it is pushed to weak coupling for $k\gg 1$. Each of the two ferromagnetic-type domains is separated from the antiferromagnetic one by a Kosterlitz-Thouless line, as depicted in Fig. 1(a). While we cannot entirely rule out the possibility of yet another domain for sufficiently large $|J_\perp|\gg J_z$, there are no indications at this point in favor of such a scenario.

Proceeding to $1/2<s<k/2-1/2$, spin-exchange anisotropy is known[16] to be a relevant perturbation at the overscreened non-Fermi-liquid fixed point for $k>4$ (for $k=4$, it is a marginal perturbation). The basin of attraction of the overscreened fixed point is therefore confined to the line $J_z=|J_\perp|>0$. The nature of the low-temperature fixed points for $J_z\neq|J_\perp|$ was never explored in detail. As shown in Secs. II and V, the system flows to a line of stable ferromagneticlike fixed points with a residual isospin-$\frac{1}{2}$ local moment both for sufficiently small $J_z>|J_\perp|$ and for sufficiently large $J_z\gg|J_\perp|>0$. The fact that both extremes share the same low-energy physics suggests that a single phase extends throughout the domain $J_z>|J_\perp|$. Further support in favor of this interpretation is provided in the Appendix for the particular case of a spin-1 impurity. As for the domain $|J_z|<|J_\perp|$, here information is confined to the weak-coupling regime, $|\rho J_\perp|\ll 1/ks$. Depending on the parity of $2s$, the system flows either to a conventional Fermi liquid with no residual degeneracy (integer $s$) or to a $k$-channel Kondo effect with an effective spin-$\frac{1}{2}$ local moment (half integer $s$). A similar picture applies to $s>1/2$ and arbitrary $k$. It remains to be seen to what extent is this behavior generic to $|J_z|<|J_\perp|$.

For $k>2$ and isotropic antiferromagnetic exchange, the two spin sizes $s=1/2$ and $s=k/2-1/2$ share the same low-energy physics. Indeed, the corresponding Kondo models are related for $J_z=J_\perp>0$ by a strong-to-weak-coupling duality. It is not surprising, then, that the overscreened fixed point shows the same stability against weak spin-exchange anisotropy for both values of $s$.[16]

A similar type of duality appears to hold also for an *XXZ* anisotropy, at least in the case where $J_z>|J_\perp|$. To illustrate this point, consider first a spin-$\frac{1}{2}$ impurity. For $s=1/2$, spin-exchange anisotropy is known to be irrelevant when the couplings $J_z>-|J_\perp|$ are weak. Hence, the system still flows to the overscreened fixed point as in the isotropic case. In contrast, the flow is diverted to a line of stable ferromagneticlike fixed points when $J_z\gg|J_\perp|>0$ is sufficiently large. For $s=k/2-1/2$, the picture is reversed. While the overscreened fixed point is still approached when $J_z\gg|J_\perp|>0$ is large, the

system flows to a line of stable ferromagneticlike fixed points when the couplings $J_z > |J_\perp|$ are sufficiently small. Indeed, one can identify the line of stable ferromagneticlike fixed points that is approached for $s=1/2$ when $J_z \gg |J_\perp|$ is large with the one that is approached for $s=k/2-1/2$ when $J_z > |J_\perp|$ is small. This leads us to speculate that the regime $J_z > |J_\perp|$ is likewise composed of two distinct domains when $s=k/2-1/2$: a non-Fermi-liquid domain that extends from large $J_z$ and encompasses the overscreened fixed point and a ferromagneticlike domain that extends from weak coupling. It remains to be seen whether a similar strong-to-weak-coupling duality applies to $|J_\perp| > |J_z|$.

All cases alluded to above pertain to an overscreened impurity. We now turn to an underscreened spin, i.e., $s > k/2$. As shown in Secs. II and V, an *XXZ* anisotropy substantially modifies the low-energy physics of $s > k/2$ both near the free-impurity fixed point and for sufficiently large $J_z \gg |J_\perp|$. The sole exception to the rule is the case $s=k/2+1/2$ with $\delta J = J_z - |J_\perp| > 0$, where an *XXZ* anisotropy has only a marginal effect in either of these limits. Consider first the range $J_z > |J_\perp|$. Here, the flow in both extremes is to the same line of ferromagneticlike fixed points with a residual isospin-$\frac{1}{2}$ local moment. As before, this suggests a single ferromagneticlike phase throughout the domain $J_z > |J_\perp|$. Similar to the case where $J_z = J_\perp > 0$, the low-energy physics is comprised of quasiparticle excitations plus a residual local moment. However, the residual degeneracy is reduced to 2, compared to $2s-k+1 > 2$ at the isotropic fixed point (for $s=k/2+1/2$, the two degeneracies are identical). This difference in degeneracies distinguishes the ferromagneticlike line of fixed points from the isotropic underscreened one.

Of the different possible cases, the most intriguing is that of an underscreened impurity with $|J_z| < |J_\perp|$ and half integer $s > 1/2$. As we have shown in Sec. II, the resulting low-energy physics is that of a $k$-channel, spin-$\frac{1}{2}$ Kondo effect, at least when the exchange couplings are sufficiently weak. Thus, an *XXZ* anisotropy drives the system from underscreened to overscreened behavior, marking a dramatic change in the low-energy physics. A more complete characterization of this exotic transition is clearly needed.

Going back to $s=1/2$, we conclude with a few final comments on the mapping of Eq. (1). We first reiterate that $J_z^*$ lies well beyond the strict range of validity of bosonization for intermediate values of $k$. Nevertheless, this approach (and its Anderson-Yuval equivalent[21]) well describes the new ferromagneticlike phase both qualitatively and quantitatively. For $k=3$, which features the largest $J_z^*$ and is thus the most prone to error, Eq. (38) is only a factor of 2 larger than the NRG estimate for a symmetric box density of states. We find this degree of agreement to be quite remarkable.

Although the mapping of Eq. (1) was derived in Sec. III for a channel-isotropic model, it can easily be extended to channel anisotropy both in the spin-flip coupling, $J_\perp \to J_{\perp n}$, and in the longitudinal coupling, $J_z \to J_{zn}$. The individual transverse couplings remain unchanged in the course of the mapping, whether isotropic or not. As for the individual longitudinal couplings, these transform according to

$$\arctan\left(\frac{\pi\rho J'_{zn}}{4}\right) = \frac{\pi}{k} + \arctan\left(\frac{\pi\rho J_{zn}}{4}\right) - 2\bar{\delta}_z, \tag{59}$$

where

$$\bar{\delta}_z = \frac{1}{k}\sum_{m=1}^{k} \arctan\left(\frac{\pi\rho J_{zm}}{4}\right) \tag{60}$$

is the average phase shift for the $k$ different channels. Accordingly, the mapping of Eqs. (59) and (60) is restricted to values of $J_{zn}$ where the modulus of the right-hand side of Eq. (59) does not exceed $\pi/2$ for any of the $k$ channels. Note that channel anisotropy is preserved by Eqs. (59) and (60), which adequately reduce to Eq. (1) in the limit of isotropic couplings.

Finally, we address the possibility of generalizing the mapping of Eq. (1) to arbitrary spin $s$. Two modifications appear when the same sequence of steps is applied to an impurity spin larger than one-half. (i) For $s > 1$, the phase shift $\delta_z$ in the absence of $J_\perp$ is a nonlinear function of $S_z$. Hence, the bosonized form of the $J_z$ interaction term is no longer linear in $S_z$ as in the case of $s=1/2$. (ii) The unitary transformation $U$ produces an additional $\Delta S_z^2$ Hamiltonian term, similar to the term generated in perturbative RG [see Eq. (12)]. For $s=1/2$, the extra term amounts to a uniform shift of the entire spectrum, which can be safely ignored. This, however, is no longer the case for $s > 1/2$, as different Kramers' doublets are split. As a result of the first modification, the mapped Hamiltonian no longer assumes the form of a simple spin-exchange interaction when $s > 1$. The case $s=1$ is an exception in this regard. Although the term $\Delta S_z^2$ is still generated by the mapping, the interaction part retains the form of a simple spin-exchange interaction. A detailed discussion of this particular case is presented in the Appendix.

## ACKNOWLEDGMENTS

Stimulating discussions with Natan Andrei, Piers Coleman, Andres Jerez, Eran Lebanon, Pankaj Mehta, and Gergely Zaránd are gratefully acknowledged. A.S. was supported in part by the Centers of Excellence Program of the Israel Science Foundation, founded by The Israel Academy of Science and Humanities. L.D.L. was supported by NSF Grant No. DMR 0312495.

## APPENDIX: EXACT MAPPING FOR $s=1$

In this appendix, we extend the mapping of Eq. (1) to a spin-1 impurity. As explained in the main text, $s=1$ is the only other spin size for which a simple spin-exchange interaction is recovered at the conclusion of the mapping. However, an additional local field proportional to $S_z^2$ is generated. The basic steps of the derivation are nearly identical to those carried out in Sec. III for $s=1/2$. Only a few minor modifications appear, as specified below.

Our starting point is the Hamiltonian of Eq. (19), where $\vec{S}$ now represents a spin-1 operator. Bosonizing the fermion fields according to Eq. (21), the bosonic Hamiltonian assumes the form of Eq. (24) with one sole variation: The longitudinal spin-exchange term now reads

$$\delta_1 \frac{a}{2\pi^2\rho}\sum_{n=1}^{k}[\nabla\Phi_{n\uparrow}(0) - \nabla\Phi_{n\downarrow}(0)]S_z, \tag{A1}$$

where

$$\delta_1 = \arctan\left(\frac{\pi\rho J_z}{2}\right). \tag{A2}$$

Converting to the boson fields of Eqs. (26) and (27) and applying the transformation $U=\exp\left[i\sqrt{\frac{8}{k}}\Phi_s(0)S_z\right]$, the transformed Hamiltonian $\mathcal{H}'=U\mathcal{H}U^\dagger$ retains the same overall form as Eq. (32), but with two important modifications. (i) The coefficient of the $\nabla\Phi_s(0)S_z$ term is replaced with

$$\left(\delta_1 - \frac{2\pi}{k}\right)\frac{a}{2\pi^2\rho}\sqrt{2k}. \tag{A3}$$

(ii) A new Hamiltonian term $\mathcal{H}_\Delta=\Delta S_z^2$ with

$$\Delta = 8D\left[\frac{1}{k} - \frac{\delta_1}{\pi}\right] \tag{A4}$$

is added to $\mathcal{H}'$.[30] Proceeding with the transformation $\Phi_s(x) \rightarrow -\Phi_s(x)$ and converting back to a fermionic representation, the Hamiltonian $\mathcal{H}'$ regains the form of Eq. (19), but with certain renormalized parameters:

$$J_z \rightarrow J_z', \tag{A5}$$

$$h \rightarrow -h, \tag{A6}$$

$$g_i \rightarrow 2g_e - g_i, \tag{A7}$$

and

$$\Delta = 0 \rightarrow 8D\left[\frac{1}{k} - \frac{\delta_1}{\pi}\right]. \tag{A8}$$

Here, $J_z'$ is determined from the equation

$$\arctan\left(\frac{\pi\rho J_z'}{2}\right) = \frac{2\pi}{k} - \arctan\left(\frac{\pi\rho J_z}{2}\right), \tag{A9}$$

which comes in place of Eq. (1) for a spin-$\frac{1}{2}$ impurity.

As for $s=1/2$, the mapping of Eqs. (A5)–(A9) is restricted to values of $J_z$ where the right-hand side of Eq. (A9) does not exceed $\pi/2$. This constrains the mapping to $k\geqslant 3$ (overscreened impurity) and $J_z \geqslant J_{\min}$, with

$$J_{\min} = \begin{cases} \dfrac{2}{\sqrt{3}\pi\rho} > 0, & k=3 \\ 0, & k=4 \\ -\dfrac{2}{\pi\rho}\tan\left(\dfrac{\pi}{2} - \dfrac{2\pi}{k}\right) < 0, & k>4. \end{cases} \tag{A10}$$

Specifically, for $k>4$, the coupling regimes $J_{\min} \leqslant J_z' < 0$ and $J_z > J_z^* > 0$, with

$$J_z^* = \frac{2}{\pi\rho}\tan\left(\frac{2\pi}{k}\right), \tag{A11}$$

are mapped onto one another. This should be compared with Eqs. (37) and (38) for $s=1/2$.

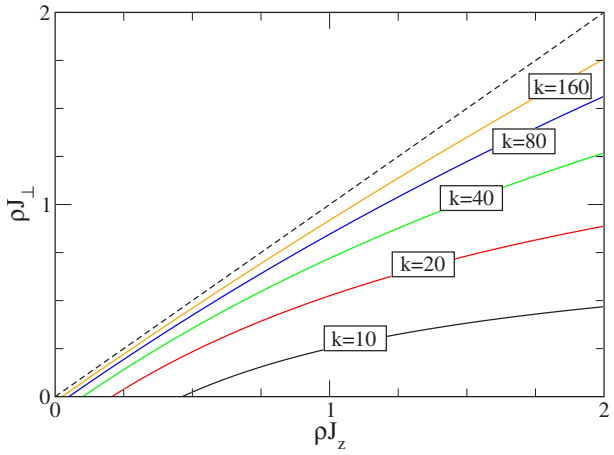


FIG. 6. (Color online) Lower bound on the basin of attraction of the line of stable ferromagneticlike fixed points for $s=1$ and different values of $k\gg 1$. In the region below and to the right of each solid line, both $\Delta<0$ and $J_z'<-|J_\perp|$. Hence, the system flows to the line of stable ferromagneticlike fixed points with a residual degeneracy of two. The fixed-point structure in the remaining portion of the domain $J_z>|J_\perp|$, i.e., in between the solid lines and the overscreened line $J_z=|J_\perp|$ (marked by a dashed line), cannot be deduced based on Eqs. (A5)–(A9) alone.

Since Eqs. (A5)–(A9) define yet another multichannel Kondo Hamiltonian with both spin-exchange anisotropy and a potentially competing $\Delta S_z^2$ term, we have no conclusive way to deduce its fixed-point structure throughout the $J_z$-$J_\perp$ plane. Nevertheless, the behavior in one particular region is clear. For values of $J_z$ where both $J_z'<-|J_\perp|$ and $\Delta<0$, the ferromagnetic spin exchange and the $\Delta S_z^2$ term conspire to favor a ferromagneticlike state with a residual twofold degeneracy. Here, the residual degeneracy stems from the $S_z^2=1$ Kramers' doublet favored by $\Delta<0$. For such values of $J_z$, one can safely conclude that the system flows to the same line of stable ferromagneticlike fixed points identified in Sec. V from the strong-coupling expansion. These considerations provide us with the following lower bound on the basin of attraction of the ferromagneticlike line of fixed points:

$$|J_\perp| < |J_{\min}|, \tag{A12}$$

$$J_z > \frac{2}{\pi\rho}\tan\left[\frac{2\pi}{k} + \arctan\left(\frac{\pi\rho|J_\perp|}{2}\right)\right]. \tag{A13}$$

Figure 6 depicts that portion of the $J_z$-$J_\perp$ plane defined by Eqs. (A12) and (A13) for several values of $k\gg 1$. With increasing $k$, a growing fraction of the domain $J_z>|J_\perp|$ is covered by this region, which stretches for $k\gg 1$ from $\rho J_z \approx 4/k \ll 1$ and upward in $J_z$. This result partially bridges between the strong- and weak-coupling limits ($\rho J_z \gg 1, |\rho J_\perp|$ and $0<|\rho J_\perp|<\rho J_z \ll 1/k$, respectively), where flow to a ferromagneticlike state has been established in Secs. II and V using vastly different techniques. As for the remaining fraction of the domain $J_z>|J_\perp|$, its fixed-point structure cannot be immediately deduced based on Eqs. (A5)–(A9) alone.

[1] D. L. Cox, Phys. Rev. Lett. **59**, 1240 (1987).
[2] C. L. Seaman, M. B. Maple, B. W. Lee, S. Ghamaty, M. S. Torikachvili, J.-S. Kang, L. Z. Liu, J. W. Allen, and D. L. Cox, Phys. Rev. Lett. **67**, 2882 (1991).
[3] D. C. Ralph and R. A. Buhrman, Phys. Rev. Lett. **69**, 2118 (1992).
[4] D. C. Ralph, A. W. W. Ludwig, J. von Delft, and R. A. Buhrman, Phys. Rev. Lett. **72**, 1064 (1994).
[5] A. Zawadowski, Phys. Rev. Lett. **45**, 211 (1980).
[6] K. Vladar and A. Zawadowski, Phys. Rev. B **28**, 1564 (1983); **28**, 1582 (1983); **28**, 1596 (1983).
[7] T. Cichorek, A. Sanchez, P. Gegenwart, F. Weickert, A. Wojakowski, Z. Henkie, G. Auffermann, S. Paschen, R. Kniep, and F. Steglich, Phys. Rev. Lett. **94**, 236603 (2005). This paper reports two-channel Kondo characteristics in transport properties of ThAsSe, presumably due to scattering off structural two-level systems.
[8] K. A. Matveev, Zh. Eksp. Teor. Fiz. **99**, 1598 (1991) [Sov. Phys. JETP **72**, 892 (1991)].
[9] D. Berman, N. B. Zhitenev, R. C. Ashoori, and M. Shayegan, Phys. Rev. Lett. **82**, 161 (1999).
[10] R. M. Potok, I. G. Rau, H. Shtrikman, Y. Oreg, and D. Goldhaber-Gordon, Nature (London) **446**, 167 (2007).
[11] For a comprehensive review of the multichannel Kondo effect, see D. L. Cox and A. Zawadovski, Adv. Phys. **47**, 599 (1998).
[12] A. Posazhennikova and P. Coleman, Phys. Rev. Lett. **94**, 036802 (2005).
[13] P. Mehta, N. Andrei, P. Coleman, L. Borda, and G. Zaránd, Phys. Rev. B **72**, 014430 (2005).
[14] P. Coleman and C. Pépin, Phys. Rev. B **68**, 220405(R) (2003).
[15] W. Koller, A. C. Hewson, and D. Meyer, Phys. Rev. B **72**, 045117 (2005).
[16] I. Affleck, A. W. W. Ludwig, H.-B. Pang, and D. L. Cox, Phys. Rev. B **45**, 7918 (1992).
[17] R. M. Konik, H. Saleur, and A. W. W. Ludwig, Phys. Rev. B **66**, 075105 (2002).
[18] O. Újsághy, A. Zawadowski, and B. L. Gyorffy, Phys. Rev. Lett. **76**, 2378 (1996).
[19] K. G. Wilson, Rev. Mod. Phys. **47**, 773 (1975).
[20] M. Fabrizio, A. O. Gogolin, and P. Noziéres, Phys. Rev. B **51**, 16088 (1995).
[21] J. Ye, Phys. Rev. Lett. **77**, 3224 (1996).
[22] A duality similar to Eq. (1) was noted in H. Yi, Phys. Rev. B **65**, 195101 (2002); however, its implications were never discussed.
[23] P. W. Anderson, J. Phys. C **3**, 2436 (1970).
[24] F. D. M. Haldane, J. Phys. C **14**, 2585 (1981).
[25] P. Noziéres and A. Blandin, J. Phys. (Paris) **41**, 193 (1980).
[26] See Eqs. (2) of Ref. 21 with $Q \to 1$.
[27] Careless truncation may result in symmetry breaking. To avoid spurious symmetry breaking in the course of truncation, it is essential to accommodate the degenerate multiplets of $\mathcal{H}_N$ in their entirety. This may require a slight increase in the number of states retained at certain iterations.
[28] In our code, we exploited the conservation of the following quantities: the total electronic charge, the $z$ component of the overall spin of the system, and the operator $L_z = \Sigma_{j=1}^{N} \Sigma_\sigma [f_{j3\sigma}^\dagger f_{j3\sigma} - f_{j1\sigma}^\dagger f_{j1\sigma}]$. We did not make use of the full SU(3) channel symmetry of the model.
[29] I. Affleck and A. W. W. Ludwig, Nucl. Phys. B **360**, 641 (1991).
[30] $\Delta$ is formally proportional to $\delta(0)$, which is regularized as $1/a$.